energies

MDPI

Article

Risk-Averse Coordinated Operation of Distributed Energy Resources in Active Distribution Networks Considering Load and Renewable Uncertainty

Samarendra Pratap Singh [1], Neeraj Kanwar [1,*], Amit Saraswat [1] and Vikash Rameshar [2,*]

[1] Department of Electrical Engineering, Manipal University Jaipur, Jaipur 303007, Rajasthan, India; samarendra.singh@jaipur.manipal.edu (S.P.S.); amit.saraswat@jaipur.manipal.edu (A.S.)
[2] Department of Electrical and Electronic Engineering Technology, University of Johannesburg, Johannesburg 2094, South Africa
* Correspondence: neeraj.kanwar@jaipur.manipal.edu (N.K.); vikashr@uj.ac.za (V.R.)

Abstract

This paper presents a risk-averse information-gap decision theory (IGDT)-based day-ahead scheduling framework for active distribution networks with high penetration of inverter-interfaced resources. The proposed day-ahead strategy coordinates active and reactive power scheduling in an active distribution network comprising renewable generation, diesel units, demand-side management, electric vehicle charging stations, and energy-storage-equipped soft open points. The corresponding deterministic operating condition is then used as the reference state for uncertainty analysis. The scheduling problem is formulated as a mixed-integer nonlinear programming (MINLP) model considering network operating constraints and voltage-dependent load characteristics. Uncertainty associated with load demand and renewable generation is addressed using the IGDT risk-averse approach to quantify admissible uncertainty. The proposed methodology is implemented on a modified IEEE 33 bus distribution system considering deterministic operation, load-demand uncertainty, renewable-generation uncertainty, and simultaneous uncertainty in both load demand and renewable generation. The optimization model is developed in GAMS and solved using the DICOPT solver. The simulation results demonstrate the capability of the proposed framework to accommodate simultaneous load-demand and renewable-generation uncertainty within a predefined operating-cost threshold while maintaining secure network operation.

Keywords: IGDT; active distribution networks; MINLP; GAMS; ESOP; BESS

Check for updates

Academic Editors: Il-Yop Chung and Tek-Tjing Lie

Received: 26 May 2026
Revised: 25 June 2026
Accepted: 29 June 2026
Published: 2 July 2026

Copyright: © 2026 by the authors. Licensee MDPI, Basel, Switzerland. This article is an open access article distributed under the terms and conditions of the Creative Commons Attribution (CC BY) license.

1. Introduction

The rapid expansion of renewable energy resources, distributed generation technologies, energy storage systems, electric vehicles, and power-electronic interfaced devices is driving a fundamental transition in distribution-system operation. As a result, conventional distribution networks are evolving into active distribution networks (ADNs) characterized by bidirectional power exchange, diversified resource portfolios, and increased controllability. While the availability of these distributed resources enhances operational capabilities, it also increases the complexity of network management by introducing additional challenges related to power balancing, voltage control, congestion mitigation, loss reduction, and secure system operation.

The growing variety of distributed resources has simultaneously expanded the flexibility available within modern distribution systems. Renewable-energy units equipped with advanced inverter functionalities can contribute both active and reactive power support, whereas energy storage systems, soft open points, and energy-storage-equipped soft open points provide additional means for regulating feeder power flows and improving network utilization. At the demand side, demand response programs and electric vehicles offer controllable flexibility through adaptive consumption and energy exchange. The coordinated utilization of these resources is increasingly regarded as an essential requirement for improving the economic efficiency, reliability, and resilience of ADNs. Nevertheless, scheduling decisions remain strongly influenced by uncertainties associated with renewable generation and load demand, particularly in systems with substantial renewable penetration and increasing electrification. Consequently, considerable research efforts have focused on developing scheduling methodologies capable of coordinating diverse flexibility resources while preserving satisfactory network performance in the presence of uncertainty.

The increasing penetration of renewable energy resources has transformed active distribution network operation from conventional energy management into a coordinated scheduling problem involving multiple distributed resources. Recent studies have demonstrated that coordinated active-reactive operation of renewable generation and energy storage systems can improve voltage regulation, reduce network losses, and enhance renewable-energy utilization [1–6]. Advancements in inverter technologies have further enabled renewable resources to provide ancillary services through controllable reactive power support, thereby strengthening their contribution to network operation. These developments have established renewable coordination as a fundamental component of modern ADN scheduling frameworks.

To improve the operational flexibility required for accommodating renewable generation, significant research attention has been devoted to network flexibility resources. Battery energy storage systems are among the most widely adopted flexibility technologies owing to their capability to perform energy arbitrage, peak shaving, renewable-energy balancing, and voltage-support functions [1–3]. Beyond conventional storage technologies, soft open points (SOPs) have emerged as effective network-control devices capable of regulating active and reactive power exchange between adjacent feeders. By enabling controllable power-flow management, SOPs improve feeder utilization, alleviate congestion, and support voltage regulation [4]. More recently, energy-storage-equipped soft open points (ESOPs) have been proposed as an extension of SOP technology, providing both spatial and temporal flexibility through coordinated power-flow control and energy storage operation [5,6]. These technologies have demonstrated considerable potential for improving renewable-energy accommodation and network controllability. Nevertheless, their operational benefits remain influenced by load characteristics and the availability of flexible demand participation.

Consequently, demand-side flexibility has become an increasingly important component of active distribution network scheduling. Demand-side management (DSM) programs have been extensively investigated as a means of reshaping load profiles, reducing peak demand, and improving renewable-energy utilization [7–9]. In parallel, the limitations associated with conventional constant-power load assumptions have encouraged the adoption of voltage-dependent load (VDL) models capable of more accurately representing consumer behavior. Existing studies have shown that load-voltage interactions can significantly influence feeder loading, voltage regulation, power losses, and optimal scheduling decisions [7–12]. The evolution of this research direction has progressively expanded from standalone voltage-dependent demand modelling toward coordinated frameworks integrating voltage-sensitive demand characteristics with network-support technologies

such as SOPs [10,11]. More recently, the simultaneous consideration of voltage-dependent demand behavior, demand-side management, and ESOP operation has demonstrated the benefits of jointly exploiting demand flexibility and network flexibility within ADN scheduling frameworks [12]. These developments indicate that realistic demand modelling and flexible demand participation play an increasingly important role in determining the operational value of distributed flexibility resources and provide a natural foundation for the integration of additional flexibility mechanisms such as electric vehicles.

Beyond conventional demand-side resources, electric vehicles have emerged as mobile flexibility assets capable of providing additional support to active distribution network operation. Early investigations primarily focused on coordinated charging strategies aimed at mitigating adverse impacts on distribution networks and reducing charging costs while accommodating growing EV penetration levels [13,14]. As the storage capability of EV batteries became increasingly recognized, subsequent studies introduced vehicle-to-grid operation, enabling electric vehicles to participate actively in energy management, peak-demand reduction, and renewable-energy balancing [15,16]. These developments transformed EVs from passive electricity consumers into distributed flexibility resources capable of supporting system operation.

Recent advances in charging infrastructure have further expanded the operational role of electric vehicles. In particular, the capability of EV chargers to independently regulate active and reactive power exchange has enabled charging stations to contribute to voltage regulation, reactive power compensation, and ancillary-service provision. Studies incorporating active-reactive EV support have demonstrated improvements in network performance, voltage stability, and operational flexibility under varying operating conditions [16–18]. Moreover, four-quadrant charging technologies allow coordinated management of both active and reactive power, thereby enhancing the ability of EV charging stations to interact with renewable resources and distribution network control devices. Despite these advances, EV flexibility is frequently investigated independently of other distributed flexibility resources, limiting the exploitation of potential synergies among renewable generation, demand-side flexibility, and network-support technologies.

Recognizing the complementary characteristics of distributed flexibility resources, recent research has progressively evolved from resource-specific scheduling strategies toward integrated flexibility frameworks. Instead of treating renewable generation, energy storage systems, demand-side resources, network-control devices, and electric vehicles (EVs) independently, coordinated scheduling approaches seek to exploit the synergistic interactions among these resources to enhance overall network performance. Studies incorporating combinations of SOPs, energy storage systems, renewable resources, and EV charging infrastructure have demonstrated improvements in operational economy, renewable energy utilization, voltage regulation, and feeder utilization [19,20]. These developments indicate that coordinated flexibility utilization can substantially improve the adaptability and operational efficiency of active distribution networks. Nevertheless, most existing formulations continue to consider only selected combinations of flexibility resources, and comprehensive scheduling frameworks simultaneously coordinating renewable active-reactive support, voltage-dependent demand behavior, demand-side management, advanced EV flexibility, and ESOP operation remain relatively limited in the literature.

Despite the operational advantages offered by coordinated flexibility resources, uncertainty remains a fundamental challenge in active distribution network scheduling. Variations in renewable-energy production, load demand, electricity-market conditions, and electric-vehicle charging behavior can substantially influence operating decisions and network performance. As distribution systems become increasingly dependent on renewable and flexible resources, uncertainty-aware scheduling has become essential for ensuring

reliable and economical operation. Several modeling frameworks have been proposed to address these challenges. Early studies primarily relied on scenario-based and uncertainty-aware scheduling approaches to evaluate the impacts of renewable generation and load demand variability on network operation [21,22]. Subsequently, robust optimization techniques were introduced to obtain solutions capable of maintaining operational feasibility under adverse realizations of uncertain parameters without requiring explicit probability distributions [23,24]. These approaches have significantly improved the resilience of active distribution networks and enhanced decision-making under uncertain operating conditions. Nevertheless, their implementation often depends on representative scenarios, statistical information, or carefully defined uncertainty descriptions, which may become difficult to obtain accurately in practical distribution systems characterized by evolving operating conditions and limited historical data.

To overcome the limitations associated with probability-dependent uncertainty models, Information Gap Decision Theory (IGDT) has emerged as an attractive non-probabilistic framework for decision-making under severe uncertainty. In contrast to uncertainty-management approaches that rely on probability distributions, representative scenarios, or predefined uncertainty descriptions, IGDT evaluates the maximum admissible uncertainty that can be accommodated while satisfying a prescribed performance requirement. This characteristic makes IGDT particularly suitable for active distribution networks where reliable statistical information is unavailable or limited. However, because IGDT is not probability-based, it does not explicitly quantify the likelihood of uncertainty realizations or the expected operating performance under uncertain conditions. Consequently, the selection of an uncertainty-management framework should be guided by both the availability of uncertainty information and the objectives of the scheduling problem. However, IGDT is an appropriate choice for evaluating the uncertainty accommodation capability of active distribution networks under predefined economic-performance requirements when probabilistic uncertainty information is limited.

Recent studies have applied IGDT to power-system scheduling problems to evaluate the trade-off between operational performance and uncertainty tolerance. Initial applications focused on renewable-rich microgrids incorporating demand response programs, energy storage systems, and electric vehicles [25]. Subsequently, IGDT-based formulations were extended to active distribution networks through coordinated scheduling of demand-side participation and electric-vehicle charging/discharging strategies under renewable-generation uncertainty [26]. More recently, IGDT has been integrated with Volt–VAr management and distributed energy resource coordination frameworks to address simultaneous renewable-generation and load-demand uncertainty [27]. These studies demonstrate the capability of IGDT to quantify the maximum uncertainty that can be accommodated while satisfying predefined operational criteria. However, the contribution of coordinated flexibility resources toward enhancing uncertainty accommodation capability within active distribution networks remains insufficiently investigated.

The literature review and comparative assessment presented in Table 1 indicate that significant progress has been achieved in renewable-energy integration, demand-side flexibility, electric-vehicle participation, soft open point technologies, and uncertainty-aware operation of active distribution networks. Nevertheless, existing studies generally coordinate only a subset of available flexibility resources and often employ simplified representations of converter-interfaced devices. Moreover, while considerable attention has been devoted to obtaining economically attractive operating schedules under uncertainty, comparatively less emphasis has been placed on quantifying network uncertainty accommodation capability and the influence of coordinated flexibility resources on admissible uncertainty limits.

Table 1. Comparative review of representative studies.

Ref.	A-R RES Coordination	VDL/DSM	Flexible Resources (BESS/SOP/ESOP)	EV Flexibility	Uncertainty Framework
[1]	AP+RP	DSM	BESS	–	–
[2]	AP+RP	–	BESS	–	–
[3]	AP+RP	DSM	BESS	–	–
[4]	AP+RP	DSM	SOP+ESS	–	Stochastic
[5]	AP+RP	–	ESOP	–	–
[6]	AP+RP	–	ESOP	–	Hybrid
[7]	–	VDL+DSM	–	–	–
[8]	AP	DSM	BESS	–	–
[9]	–	DSM	BESS	G2V	–
[10]	AP+RP	VDL	SOP	–	–
[11]	AP+RP	VDL	SOP	–	–
[12]	AP+RP	VDL+DSM	ESOP	–	–
[13]	–	–	–	G2V	Probabilistic
[14]	–	–	–	G2V	–
[15]	AP	–	BESS	G2V/V2G	–
[16]	–	–	–	G2V/V2G+ Q	–
[17]	–	–	–	4Q (P-Q)	–
[18]	–	–	–	4Q (P-Q)	Probabilistic
[19]	AP+RP	–	SOP+ESS	G2V/V2G	–
[20]	AP+RP	–	SOP	G2V/V2G	DRO
[21]	AP	DSM	BESS	–	Scenario-Based
[22]	AP+RP	DSM	BESS	–	Uncertainty-Aware
[23]	AP+RP	–	SOP	–	Robust
[24]	AP+RP	–	–	–	Robust
[25]	AP	DSM	BESS	G2V/V2G	Stochastic and IGDT
[26]	AP+RP	DSM	BESS	G2V/V2G	IGDT
[27]	AP+RP	DSM	BESS	–	IGDT

Abbreviations: A-R RES: Coordinated active and reactive power scheduling; AP: Active power support/scheduling; RP: Reactive power support/scheduling; 4Q (P-Q): Four-quadrant active-reactive EV operation; DRO: Distributionally Robust Optimization.

To address these limitations, a unified scheduling and uncertainty-assessment framework for active distribution networks is developed in this work, with the principal contributions summarized as follows:

- A comprehensive day-ahead scheduling framework is developed for active distribution networks that simultaneously coordinates renewable energy resources, distributed generation units, voltage-dependent demand models, demand-side management programs, four-quadrant operation of EVs, and energy-storage-equipped soft open points.
- Converter-loss-aware models are incorporated for renewable-energy interfaces, EV chargers, and ESOP converters, enabling a more realistic representation of active and reactive power exchanges and their influence on network operation.
- A risk-averse Information Gap Decision Theory framework is formulated to quantify the maximum admissible uncertainty associated with renewable generation and load demand while satisfying a predefined economic-performance requirement.
- An admissible load–renewable uncertainty frontier is established to characterize the trade-off between renewable-generation uncertainty and load-demand uncertainty. The impacts of electricity-price variation, EV participation levels, demand-side flexibility, and ESOP size on load and renewable uncertainty accommodation are further investigated.

2. Mathematical Modelling and Formulation of the Optimization Framework

The operation of the active distribution network (ADN) is formulated as a day-ahead optimization problem that coordinates distributed energy resources and flexible demand to achieve economical operation. The formulation includes an objective function together with power-flow, grid-interaction, generation, storage, electric-vehicle, and load constraints to ensure feasible network operation over the scheduling horizon.

2.1. Objective Function

The objective of the proposed scheduling framework is to minimize the total operating cost of ADN. Equations (1)–(9) define the total cost function together with its individual operating-cost components. Equation (1) minimizes the total operating cost J^{tot}, comprising the utility-grid exchange cost J^{grid}, diesel-generator operating cost J^{DG}, demand-side management cost J^{DSM}, and electric-vehicle scheduling cost J^{EV}.

$$min\ J^{tot} = J^{grid} + J^{DG} + J^{DSM} + J^{EV} \tag{1}$$

Equation (2) evaluates the cost of active- and reactive-power exchange with the utility grid using prices λ_t^P and λ_t^Q, and exchanged powers P_t^{grid} and Q_t^{grid}, where $\lambda_t^Q = k_q^{EG}\lambda_t^P$ [28].

$$J^{grid} = \sum_{t\epsilon\mathcal{T}}\left[\lambda_t^P P_{i,t}^{grid} + \lambda_t^Q Q_{i,t}^{grid}\right] \tag{2}$$

Equations (3)–(7) describe the operating cost and commitment model of DGs. Equation (3) aggregates the active-power generation cost $C_{g,t}^P$, reactive-power support cost $C_{g,t}^Q$, and unit-transition costs $C_{g,t}^{SU}$ and $C_{g,t}^{SD}$ of DG operation. Equation (4) expresses the DG active-power generation cost using coefficients α_g, β_g, and γ_g, together with active-power output $P_{g,t}^{DG}$. Equation (5) represents an availability-based cost for reactive-power support within the minimum and maximum power-factor limits of the DG. Equation (6) models start-up and shut-down costs through coefficients C_g^{SU} and C_g^{SD}, while $\sigma_{g,t}^{SU}$ and $\sigma_{g,t}^{SD}$ denote the corresponding binary transition variables. Equation (7) restricts DG active-power output $P_{g,t}^{DG}$ within the operating limits P_g^{min} and P_g^{max} according to commitment status $u_{g,t}$.

$$J^{DG} = \sum_{t\epsilon\mathcal{T}}\sum_{g\epsilon\mathcal{G}}\left(C_{g,t}^P + C_{g,t}^Q + C_{g,t}^{SU} + C_{g,t}^{SD}\right) \tag{3}$$

$$C_{g,t}^P = \alpha_g + \beta_g P_{g,t}^{DG} + \gamma_g\left(P_{g,t}^{DG}\right)^2 \tag{4}$$

$$C_{g,t}^Q = \lambda_t^{DG} u_{g,t} \tag{5}$$

$$C_{g,t}^{SU} + C_{g,t}^{SD} = C_g^{SU}\Omega_{g,t}^{SU} + C_g^{SD}\Omega_{g,t}^{SD} \tag{6}$$

$$u_{g,t}P_g^{min} \le P_{g,t}^{DG} \le u_{g,t}P_g^{max} \tag{7}$$

For inverter-based renewable resources and EV charging infrastructure, the effect of reactive-power support is reflected indirectly through converter-loss models that depend on both active and reactive power transfer. An increase in reactive-power output is generally accompanied by additional converter losses, which may marginally reduce the net active-power contribution delivered to the network. Likewise, EV chargers operating in reactive-power support mode may require a small increase in energy exchange to satisfy the specified battery charging requirements. As a result, reactive-power provision can indirectly influence the total energy requirement and operating cost of the distribution network.

Equation (8) quantifies the cost associated with demand-side management using the compensation coefficient ψ_i and the downward active-power adjustment $\Delta P_{i,t}^{-}$. Equation (9) represents the electric-vehicle scheduling cost using electricity price λ_t^P and charging-station active power $P_{s,t}^{EV}$. Collectively, these equations establish the economic objective for day-ahead scheduling of generation resources, flexible demand, and electric-vehicle charging activities.

$$J^{DSM} = \sum_{t \epsilon \mathcal{T}} \sum_{i \epsilon \mathcal{N}} \psi_i \Delta P_{i,t}^{-} \tag{8}$$

$$J^{EV} = \sum_{t \epsilon \mathcal{T}} \sum_{s \epsilon \mathcal{S}} \lambda_t^P P_{s,t}^{EV} \tag{9}$$

2.2. Power Flow Constraint

Equations (10)–(13) define the AC power-flow relationships of the active distribution network. Equations (10) and (11) establish the nodal active- and reactive-power balance using injected powers $P_{i,t}^{inj}$ and $Q_{i,t}^{inj}$, load demands $P_{i,t}^{L}$ and $Q_{i,t}^{L}$, and branch power flows $P_{ij,t}$ and $Q_{ij,t}$. Equations (12)–(13) describe active-power flow $P_{ij,t}$ and reactive-power flow $Q_{ij,t}$ between interconnected buses as functions of bus-voltage magnitudes $V_{i,t}$ and $V_{j,t}$, voltage-angle difference $\theta_{i,t} - \theta_{j,t}$, and line-admittance parameters G_{ij} and B_{ij}. These equations establish the AC power-flow relationships governing network operation.

$$P_{i,t}^{inj} - P_{i,t}^{L} = \sum_{j \epsilon \Omega} P_{ij,t} \tag{10}$$

$$Q_{i,t}^{inj} - Q_{i,t}^{L} = \sum_{j \epsilon \Omega} Q_{ij,t} \tag{11}$$

$$P_{ij,t} = V_{i,t}^2 G_{ij} - V_{i,t} V_{j,t} \left[G_{i,j} \cos\left(\theta_{i,t} - \theta_{j,t}\right) + B_{ij} \sin\left(\theta_{i,t} - \theta_{j,t}\right) \right] \tag{12}$$

$$Q_{ij,t} = -V_{i,t}^2 B_{ij} - V_{i,t} V_{j,t} \left[G_{i,j} \sin\left(\theta_{i,t} - \theta_{j,t}\right) - B_{ij} \cos\left(\theta_{i,t} - \theta_{j,t}\right) \right] \tag{13}$$

2.3. External Grid and Voltage Constraint

The external-grid and voltage-security constraints are represented by Equations (14)–(21). Equations (14) and (15) limit active-power exchange $P_{i,t}^{grid}$ and reactive-power exchange $Q_{i,t}^{grid}$ with the utility grid to their allowable operating ranges. Equations (16)–(19) decompose reactive-power exchange into import $Q_{i,t}^{imp}$ and export $Q_{i,t}^{exp}$ components, prohibit their simultaneous occurrence, and impose the corresponding exchange limits. Equation (20) specifies the voltage magnitude of the slack bus $V_{r,t}$, while Equation (21) maintains the nodal voltage magnitude $V_{i,t}$ within the allowable voltage limits V^{min} and V^{max}.

$$P^{grid,min} \leq P_{i,t}^{grid} \leq P^{grid,max} \tag{14}$$

$$Q^{grid,min} \leq Q_{i,t}^{grid} \leq Q^{grid,max} \tag{15}$$

$$Q_{i,t}^{grid} = Q_{i,t}^{imp} - Q_{i,t}^{exp} \tag{16}$$

$$Q_{i,t}^{imp} . Q_{i,t}^{exp} = 0 \tag{17}$$

$$0 \leq Q_{i,t}^{imp} \leq Q_{i}^{imp,max} \tag{18}$$

$$0 \leq Q_{i,t}^{exp} \leq Q_{i}^{exp,max} \tag{19}$$

$$V_{r,t} = 1.0 \tag{20}$$

$$V^{min} \leq V_{i,t} \leq V^{max} \tag{21}$$

2.4. Diesel Generator Constraints

The DG operating limits are represented by Equations (22)–(24). Equation (22) specifies the allowable active-power generation range, while Equation (23) constrains reactive-power support according to the prescribed power-factor limits. Finally, Equation (24) ensures that the apparent power associated with the DG output remains within its rated capacity. These constraints capture the practical operating limits of DGs within the ADN.

$$u_{g,t}P_g^{min} \le P_{g,t}^{DG} \le u_{g,t}P_g^{max} \tag{22}$$

$$-P_{g,t}^{DG}\tan\left(\varnothing_g^{max}\right) \le Q_{g,t}^{DG} \le P_{g,t}^{DG}\tan\left(\varnothing_g^{max}\right) \tag{23}$$

$$\left(P_{g,t}^{DG}\right)^2 + \left(Q_{g,t}^{DG}\right)^2 \le \left(S_{g,t}^{DG}\right)^2 \tag{24}$$

2.5. Renewable Energy Sources Constraints

The RES model is represented by Equations (25)–(27), which describe the operation of the grid-side converter (GSC). Equation (25) relates available renewable generation $P_{r,t}^{av}$ to AC-side active-power injection $P_{r,t}^{ac}$ and converter losses $P_{r,t}^{loss}$. Equation (26) expresses converter losses as a function of the apparent power transferred through the GSC by considering active-power output $P_{r,t}^{ac}$ and reactive-power output $Q_{r,t}^{ac}$. Finally, Equation (27) limits converter operation according to the apparent-power capability $S_{r,t}^{ac}$.

$$P_{r,t}^{av} = P_{r,t}^{ac} + P_{r,t}^{loss} \tag{25}$$

$$P_{r,t}^{loss} = \eta_r\sqrt{\left(P_{r,t}^{ac}\right)^2 + \left(Q_{r,t}^{ac}\right)^2} \tag{26}$$

$$\left(P_{r,t}^{ac}\right)^2 + \left(Q_{r,t}^{ac}\right)^2 \le \left(S_{r,t}^{ac}\right)^2 \tag{27}$$

2.6. Energy-Storage-Equipped Soft Open Point Constraints

An ESOP, shown in Figure 1, comprises two back-to-back voltage-source converters (VSCs) connected through a DC link with an integrated battery energy storage system (BESS). This arrangement enables power exchange between feeders while providing energy-shifting capability through the storage unit.

The ESOP model is described by Equations (28)–(39). Equation (28) establishes the active-power balance involving converter power exchanges $P_{e,t}^{(x)}$ and $Q_{e,t}^{(x)}$, converter losses $P_{e,t}^{loss,1}$ and $P_{e,t}^{loss,2}$, and net BESS power $P_{b,t}^{net}$. Equations (29) and (30) evaluate converter losses from the active-power components $P_{e,t}^{(x)}$ and $P_{e,t}^{(y)}$, reactive-power components $Q_{e,t}^{(x)}$ and $Q_{e,t}^{(y)}$, and converter loss coefficient ξ_e. Equation (31) relates the net BESS power to the charging power $P_{b,t}^{ch}$ and discharging power $P_{b,t}^{dis}{}^{dis}$. Equations (32) and (33) define the converter apparent-power capability $S_{e,t}^{max}$. Equation (34) describes the evolution of BESS SOC considering charging and discharging efficiencies $\eta_{b,t}^{ch}$ and $\eta_{b,t}^{dis}$, while Equations (35)–(37) impose the associated charging and discharging constraints using binary variables $u_{b,t}^{ch}$ and $u_{b,t}^{dis}$. Finally, Equations (38) and (39) specify the permissible SOC range together with the cyclic operating requirement. These equations collectively represent the coordinated operation of the ESOP and BESS within the proposed optimization framework.

$$P_{e,t}^{(x)} + P_{e,t}^{(y)} + P_{e,t}^{loss,1} + P_{e,t}^{loss,2} + P_{b,t}^{net} = 0 \tag{28}$$

$$P_{e,t}^{loss,1} = \xi_e\sqrt{\left(P_{e,t}^{(x)}\right)^2 + \left(Q_{e,t}^{(x)}\right)^2} \tag{29}$$

$$P_{e,t}^{loss,2} = \xi_e \sqrt{\left(P_{e,t}^{(y)}\right)^2 + \left(Q_{e,t}^{(y)}\right)^2} \tag{30}$$

$$P_{b,t}^{net} = P_{b,t}^{ch} - P_{b,t}^{dis} \tag{31}$$

$$\left(P_{e,t}^{(x)}\right)^2 + \left(Q_{e,t}^{(x)}\right)^2 \le \left(S_{e,t}^{max}\right)^2 \tag{32}$$

$$\left(P_{e,t}^{(y)}\right)^2 + \left(Q_{e,t}^{(y)}\right)^2 \le \left(S_{e,t}^{max}\right)^2 \tag{33}$$

$$SoC_{b,t} = SoC_{b,t-1} + \eta_{b,t}^{ch} P_{b,t}^{ch} - \frac{P_{b,t}^{dis}}{\eta_{b,t}^{dis}} \tag{34}$$

$$u_{b,t}^{ch} + u_{b,t}^{dis} \le 1 \tag{35}$$

$$0 \le P_{b,t}^{ch} \le u_{b,t}^{ch} P_b^{ch,max} \tag{36}$$

$$0 \le P_{b,t}^{dis} \le u_{b,t}^{dis} P_b^{dis,max} \tag{37}$$

$$SoC_b^{min} \le SoC_{b,t} \le SoC_b^{max} \tag{38}$$

$$SoC_{b,T}^{final} = SoC_{b,0}^{init} \tag{39}$$

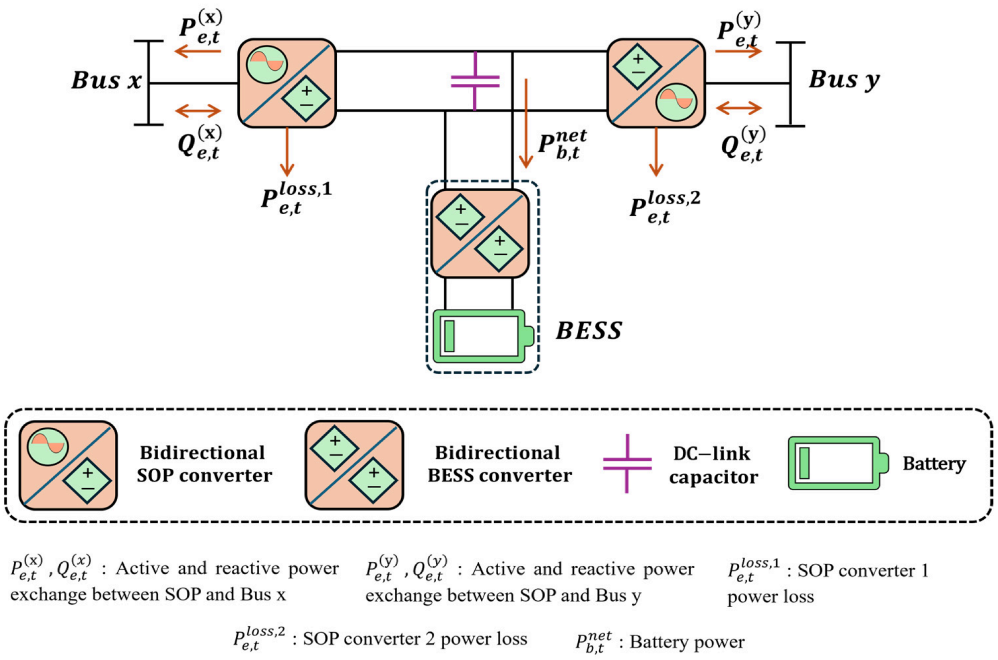


Figure 1. Schematic diagram of ESOP.

2.7. Electric Vehicle Constraints

The EV model is represented by Equations (40)–(50), which describe battery energy dynamics, converter operation, charging and discharging limits, and charging-station aggregation. Equations (40)–(42) define the energy state of the EV battery through arrival energy E_v^{arr}, battery energy $E_{v,t}$, and required departure energy E_v^{req}. Equation (43) bounds the EV battery energy $E_{v,t}$ within the permissible operating range defined by E_v^{min} and E_v^{max}. Equation (44) establishes the power balance between grid-side power $P_{v,t}^{grid}$, battery power $P_{v,t}^{bat}$, and converter losses $P_{v,t}^{loss}$. Equation (45) evaluates converter losses $P_{v,t}^{loss}$ as a function of active-power exchange $P_{v,t}^{grid}$ and reactive-power exchange $Q_{v,t}^{grid}$. Equation (46) constrains active and reactive power exchange within the converter capability S_v^{max}. Equation (47) imposes charging and vehicle-to-grid (V2G) discharging limits

through $P_v^{ch,max}$ and $P_v^{dis,max}$, while Equation (48) permits power exchange only during the connection period T_v^{conn}. Finally, Equations (49) and (50) aggregate individual EV active and reactive power contributions to obtain charging-station power injections $P_{s,t}^{EV}$ and $Q_{s,t}^{EV}$. These equations describe the energy management and grid-interaction behavior of EVs connected to the charging infrastructure.

$$E_{v,t_a} = E_v^{arr} \tag{40}$$

$$E_{v,t} = E_{v,t-1} + P_{v,t}^{bat} \tag{41}$$

$$E_{v,t_d} = E_v^{req} \tag{42}$$

$$E_v^{min} \le E_{v,t} \le E_v^{max} \tag{43}$$

$$P_{v,t}^{grid} = P_{v,t}^{bat} + P_{v,t}^{loss} \tag{44}$$

$$P_{v,t}^{loss} = \mu_{vr}\left|P_{v,t}^{grid}\right| + \mu_{vi}\left|Q_{v,t}^{grid}\right| \tag{45}$$

$$\left(P_{v,t}^{grid}\right)^2 + \left(Q_{v,t}^{grid}\right)^2 \le (S_v^{max})^2 \tag{46}$$

$$-P_v^{dis,max} \le P_{v,t}^{grid} \le P_v^{ch,max} \tag{47}$$

$$P_{v,t}^{grid} = 0 \quad \forall t \notin \mathcal{T}_v^{conn} \tag{48}$$

$$P_{s,t}^{EV} = \sum_{v \in \mathcal{V}_s} P_{v,t}^{grid} \tag{49}$$

$$Q_{s,t}^{EV} = \sum_{v \in \mathcal{V}_s} Q_{v,t}^{grid} \tag{50}$$

2.8. Voltage-Dependent Load Modelling and DSM Constraints

The load model is represented by Equations (51)–(59), which describe voltage-dependent demand characteristics and demand-side management (DSM) flexibility in the ADN. Equations (51) and (52) determine the active and reactive fixed-load $P_{i,t}^F$ and $Q_{i,t}^F$ from nominal load values $P_i^{F,0}$ and $Q_i^{F,0}$ using voltage-sensitivity exponents λ_i^P and λ_i^Q. Equations (53) and (54) define the active and reactive shiftable-load $P_{i,t}^S$ and $Q_{i,t}^S$ by incorporating DSM adjustments $\Delta P_{i,t}^+$, $\Delta P_{i,t}^-$, $\Delta Q_{i,t}^+$, and $\Delta Q_{i,t}^-$. Equation (55) links reactive-power adjustments to active-power shifting through the load power-factor angle ϕ_i. Equation (56) limits the allowable DSM actions according to the participation factor η_i, while Equation (57) prevents simultaneous upward and downward load shifting. Equation (58) enforces energy neutrality by requiring the cumulative upward and downward load adjustments to remain equal over the scheduling horizon. Finally, Equation (59) selects either fixed-load $P_{i,t}^F$ and $Q_{i,t}^F$ or shiftable-load $P_{i,t}^S$ and $Q_{i,t}^S$ to obtain the load demand $P_{i,t}^L$ and $Q_{i,t}^L$. These equations capture voltage-sensitive load behavior and DSM-enabled demand flexibility in the distribution network.

$$P_{i,t}^F = P_i^{F,0}\left(\frac{V_{i,t}}{V^0}\right)^{\lambda_i^P} \tag{51}$$

$$Q_{i,t}^F = Q_i^{F,0}\left(\frac{V_{i,t}}{V^0}\right)^{\lambda_i^Q} \tag{52}$$

$$P_{i,t}^S = \left(P_{i,t}^{S,0} + \Delta P_{i,t}^+ - \Delta P_{i,t}^-\right)\left(\frac{V_{i,t}}{V^0}\right)^{\lambda_i^P} \tag{53}$$

$$Q_{i,t}^S = \left(Q_{i,t}^{S,0} + \Delta Q_{i,t}^+ - \Delta Q_{i,t}^-\right)\left(\frac{V_{i,t}}{V^0}\right)^{\lambda_i^Q} \tag{54}$$

$$\Delta Q_{i,t}^{+} = \Delta P_{i,t}^{+}\tan(\phi_i), \quad \Delta Q_{i,t}^{-} = \Delta P_{i,t}^{-}\tan(\phi_i) \tag{55}$$

$$0 \le \Delta P_{i,t}^{+} \le \eta_i P_{i,t}^{S,0}, \quad 0 \le \Delta P_{i,t}^{-} \le \eta_i P_{i,t}^{S,0} \tag{56}$$

$$\Delta P_{i,t}^{+}.\Delta P_{i,t}^{-} = 0 \tag{57}$$

$$\sum_{t\in\mathcal{T}} \Delta P_{i,t}^{+} = \sum_{t\in\mathcal{T}} \Delta P_{i,t}^{-} \tag{58}$$

$$P_{i,t}^{L} = \chi_n P_{i,t}^{F} + (1-\chi_n) P_{i,t}^{S}, \quad Q_{i,t}^{L} = \chi_n Q_{i,t}^{F} + (1-\chi_n) Q_{i,t}^{S} \tag{59}$$

2.9. Risk-Averse IGDT-Based Uncertainty Assessment

The deterministic scheduling model represented by Equations (1)–(59) is first solved using forecasted load-demand and renewable-generation profiles. The resulting optimal operating cost is denoted by $J^{tot,det}$, where $J^{tot,det}$ represents the deterministic total operating cost obtained from Equation (1). In practical distribution-system operation, forecasting errors associated with load demand and renewable generation may influence network operation and scheduling decisions. To evaluate the capability of the proposed scheduling framework to accommodate such uncertainties, a risk-averse Information Gap Decision Theory (IGDT) approach is adopted.

Unlike stochastic and robust optimization approaches that require probabilistic information or predefined uncertainty descriptions, IGDT determines the maximum admissible uncertainty that can be tolerated while satisfying a specified performance requirement. In this study, the performance requirement is represented by an allowable increase in operating cost relative to the deterministic solution. Let α^L and α^R denote the uncertainty radii associated with load demand and renewable generation, respectively.

Since the voltage-dependent load model defined by Equations (51)–(59) is formulated using nominal fixed-load and shiftable-load components, load uncertainty is imposed directly on these nominal demand levels. Accordingly, Equations (51)–(54) are modified as follows:

$$P_{i,t}^{F,U} = P_i^{F,0}(1+\alpha^L)\left(\frac{V_{i,t}}{V^0}\right)^{\lambda_i^P} \tag{60}$$

$$Q_{i,t}^{F,U} = Q_i^{F,0}(1+\alpha^L)\left(\frac{V_{i,t}}{V^0}\right)^{\lambda_i^Q} \tag{61}$$

$$P_{i,t}^{S,U} = \left(P_{i,t}^{S,0}\left(1+\alpha^L\right) + \Delta P_{i,t}^{+} - \Delta P_{i,t}^{-}\right)\left(\frac{V_{i,t}}{V^0}\right)^{\lambda_i^P} \tag{62}$$

$$Q_{i,t}^{S,U} = \left(Q_{i,t}^{S,0}\left(1+\alpha^L\right) + \Delta Q_{i,t}^{+} - \Delta Q_{i,t}^{-}\right)\left(\frac{V_{i,t}}{V^0}\right)^{\lambda_i^Q} \tag{63}$$

$P_{i,t}^{F,U}$ and $Q_{i,t}^{F,U}$ denote the uncertain active and reactive fixed-load components, respectively, while $P_{i,t}^{S,U}$ and $Q_{i,t}^{S,U}$ represent the uncertain active and reactive shiftable-load components. The corresponding uncertain load demand is obtained as follows:

$$P_{i,t}^{L,U} = \chi_n P_{i,t}^{F,U} + (1-\chi_n) P_{i,t}^{S,U} \tag{64}$$

$$Q_{i,t}^{L,U} = \chi_n Q_{i,t}^{F,U} + (1-\chi_n) Q_{i,t}^{S,U} \tag{65}$$

where $P_{i,t}^{L,U}$ and $Q_{i,t}^{L,U}$ denote the uncertain active and reactive demands, respectively.

Renewable-generation uncertainty is represented through variations in the available renewable power defined by Equation (25). Accordingly, the renewable-energy model is modified as follows:

$$P_{r,t}^{av,U} = P_{r,t}^{av}\left(1-\alpha^R\right) \tag{66}$$

$$P_{r,t}^{av,U} = P_{r,t}^{ac,U} + P_{r,t}^{loss,U} \tag{67}$$

$$P_{r,t}^{loss,U} = \eta_r \sqrt{\left(P_{r,t}^{ac,U}\right)^2 + \left(Q_{r,t}^{ac,U}\right)^2} \tag{68}$$

$$\left(P_{r,t}^{ac,U}\right)^2 + \left(Q_{r,t}^{ac,U}\right)^2 \leq \left(S_{r,t}^{ac}\right)^2 \tag{69}$$

where $P_{r,t}^{av,U}$ denotes uncertain renewable-power availability, $P_{r,t}^{ac,U}$ denotes uncertain AC-side active-power output, and $P_{r,t}^{loss,U}$ represents converter losses under uncertain operating conditions.

Let σ denote the allowable operating-cost deviation factor. The maximum permissible operating cost under uncertainty is denoted by J^{max} and is defined as follows:

$$J^{max} = (1+\sigma) J^{tot,det} \tag{70}$$

where $J^{tot,U}$ denotes the total operating cost under uncertainty. The risk-averse performance requirement is expressed as follows:

$$J^{tot,U} \leq J^{max} \tag{71}$$

or equivalently

$$J^{tot,U} \leq (1+\sigma) J^{tot,det} \tag{72}$$

2.9.1. Load-Demand Uncertainty Assessment

For load-demand uncertainty analysis, the admissible load-uncertainty radius is obtained by solving the following:

$$\max \alpha^L \tag{73}$$

subject to the economic-performance requirement defined by Equation (72) and all operational constraints represented by Equations (1)–(65).

2.9.2. Renewable-Generation Uncertainty Assessment

For renewable-generation uncertainty analysis, the admissible renewable-generation uncertainty radius is obtained by solving the following:

$$\max \alpha^R \tag{74}$$

subject to the economic-performance requirement defined by Equation (72), all operational constraints represented by Equations (1)–(59) and Equations (66)–(69).

2.9.3. Simultaneous Load and Renewable Uncertainty Assessment

The simultaneous uncertainty assessment follows the renewable-generation uncertainty formulation presented in Section 2.9.2 with the additional fixed load-uncertainty constraint.

$$\alpha^L = \bar{\alpha}^L \tag{75}$$

where $\bar{\alpha}^L$ denotes a specified load-uncertainty level. By progressively varying $\bar{\alpha}^L$, the admissible load–renewable uncertainty frontier is obtained under the same economic-performance requirement. The resulting load–renewable uncertainty frontier characterizes the uncertainty accommodation capability of the active distribution network and enables assessment of the impacts of electricity-price variation, EV participation levels, and demand-side flexibility on network robustness.

3. Results & Discussion

3.1. System Description and Input Data

The risk-averse scheduling framework is evaluated on the standard IEEE 33-bus radial distribution system introduced by Baran and Wu [29]. The network consists of 33 buses and 32 radial branches operating at a nominal voltage level of 12.66 kV, supplying approximately 3.72 MW and 2.3 MVAr of active and reactive demand, respectively, under base operating conditions. The original feeder configuration and electrical parameters are retained, while additional distributed resources and controllable assets are integrated to enhance operational flexibility. The modified network configuration is illustrated in Figure 2.

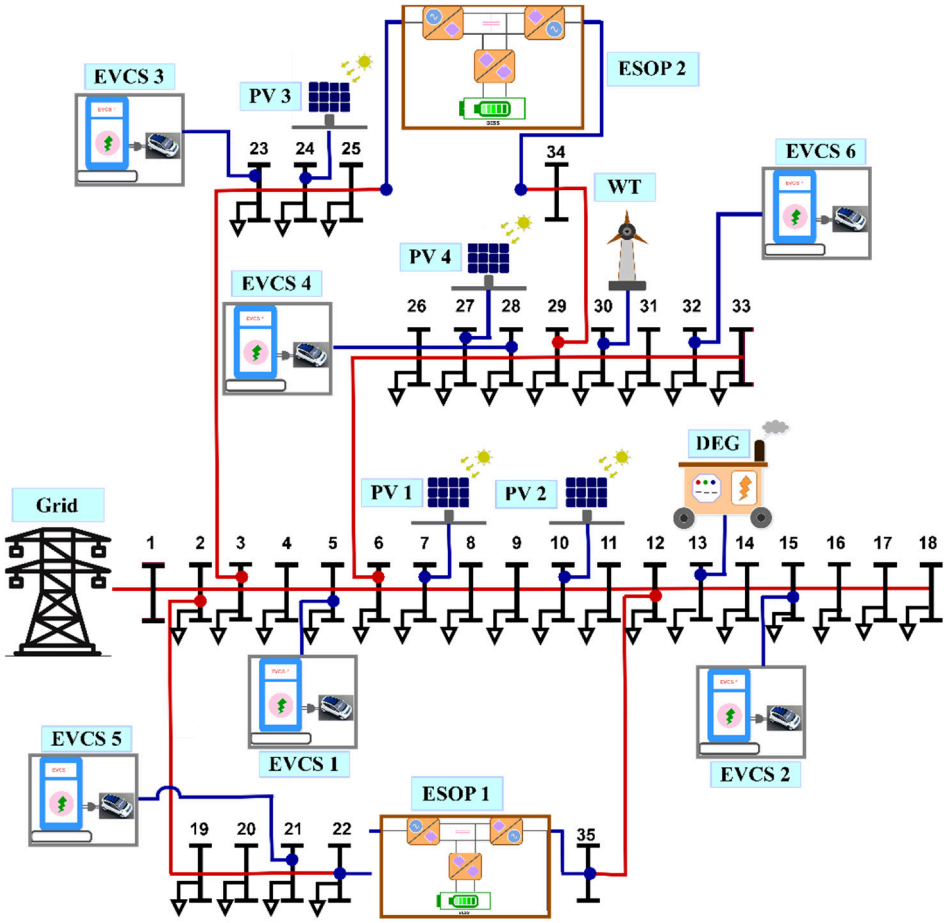


Figure 2. Network layout of the modified IEEE 33-bus system.

System demand is represented using a voltage-dependent exponential load model. Residential, industrial and commercial demands are separately considered, and each category is divided into fixed and shiftable portions to capture demand flexibility. Bus-wise load classification and the corresponding exponential coefficients are summarized in Table 2, while the composite daily demand profiles of the three consumer classes are shown in Figure 3. A load-decrement cost of \$5 is assigned to the shiftable residential segment and \$10 to the shiftable industrial and commercial segments [12]. The time-varying grid electricity price adopted in this study is shown in Figure 4, while the reactive power price is assumed as 5% of the corresponding active power tariff.

Table 2. Bus-wise load classification and voltage-dependent load parameters [30].

Load Class	Fixed Load Buses	Shiftable Load Buses	Active Power Coefficient	Reactive Power Coefficient
Residential	1, 2, 5, 6, 7, 9, 10, 11, 12, 15	3, 4, 8, 13, 14	0.18	6.0
Industrial	23, 26, 27	24, 25, 28, 29	0.92	4.04
Commercial	16, 17, 18, 21, 22, 30, 32, 33	19, 20, 31	1.51	3.40

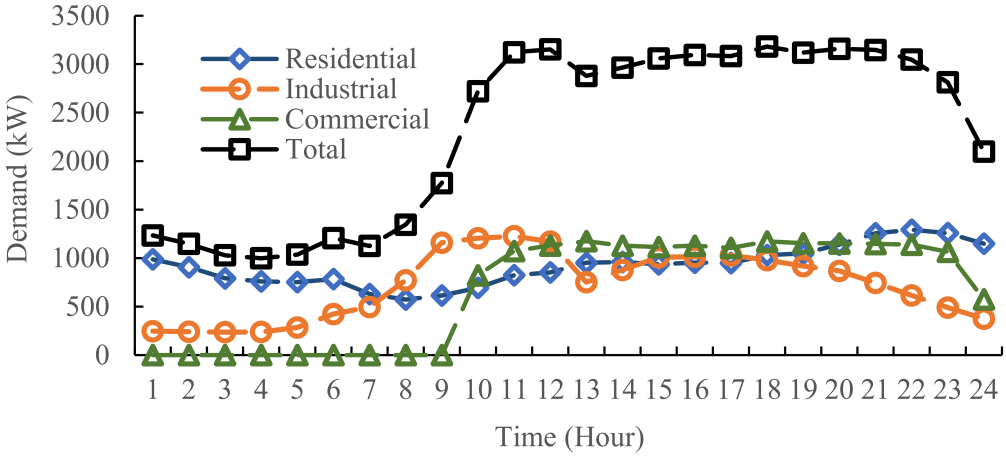


Figure 3. Composite daily demand characteristics of consumer loads [31].

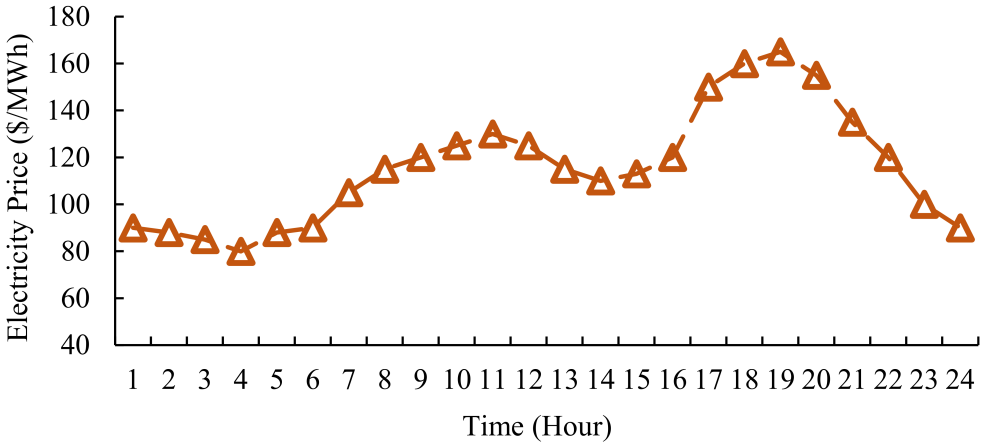


Figure 4. Time-varying grid electricity price profile [32].

The modified system further incorporates four photovoltaic units, one wind turbine generator, one diesel generator, two battery-integrated ESOP links, and six electric vehicle charging stations (EVCS). Renewable generation follows time-varying 24-h power availability profiles, as shown in Figure 5. The diesel generator installed at Bus 13 operates within a 0.95 lead–lag power-factor range, and its operating cost includes a fixed cost of \$10/h, a variable energy cost of \$75/MWh, an incremental cost of \$60/MWh^2, and start-up/shut-down costs of \$15 and \$10, respectively. Each charging station accommodates 30 EVs, comprising Nissan Leaf, Ford F-150, and Lucid Air models in proportions of 9, 9, and 12 vehicles, respectively. The ratings, locations, and operational characteristics of the distributed assets are summarized in Table 3.

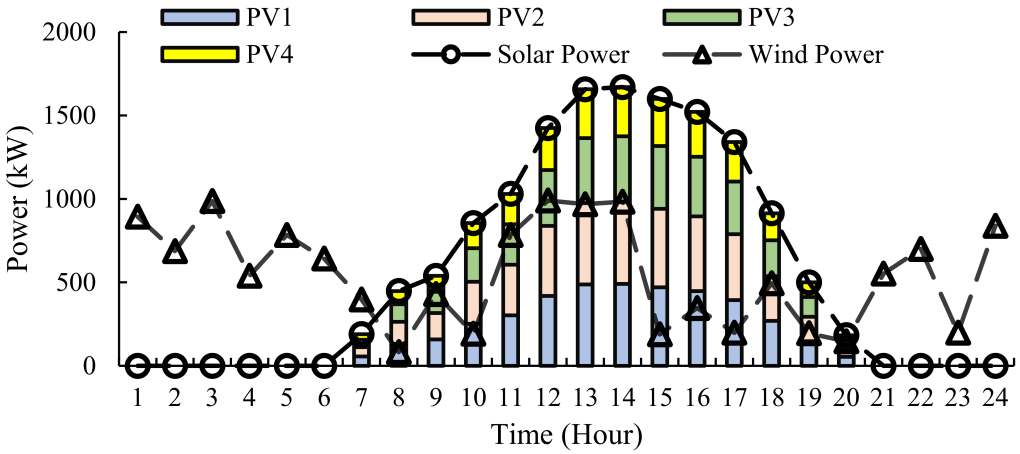


Figure 5. Available solar and wind power profiles [4].

Table 3. Distributed assets and technical specifications.

Attribute	PV Units (PV1–PV4)	WT	DEG	ESOP	BESS	EVCS
Installation Bus	7, 10, 24, 27	30	13	22–35, 25–34	Integrated with ESOPs	5, 15, 23, 28, 21, 32
Rating/Operational Characteristics	500, 500, 400, 300 kW	1000 kW	750 kW; 0.95 lead–lag PF	500 kVA bidirectional converter; loss coefficient 0.02	1000 kWh; 250 kW charge–discharge rating; 0.95 p.u. efficiency	30 EVs/station; bidirectional charging

EV charging behavior is represented through probabilistic mobility characteristics. Arrival and departure times are modelled using normal distributions expressed in 24-h format, while the initial and departure state-of-charge (SoC) requirements are represented through uniform distributions. The technical specifications of the EV models are listed in Table 4, and the EV mobility parameters are provided in Table 5. The arrival and required departure SoC levels are modelled using uniform distributions of $U(0.2, 0.4)$ p.u. and $U(0.8, 1.0)$ p.u., respectively.

Table 4. Technical specifications of EV models.

EV Model	Charger Rating (kVA)	Charging Power (kW)	Discharging Power (kW)	Battery Capacity (kWh)
Nissan Leaf	6.6	3.3	3.3	24
Ford F-150	19.2	11.3	9.6	98
Lucid Air	19.2	19.2	9.6	88

Table 5. EV Mobility parameters.

EVCS Group	Arrival Distribution (h)	Departure Distribution (h)
EVCS-1 and EVCS-2	N (20, 2.5)	N (8, 2.5)
EVCS-3 and EVCS-4	N (10, 2.5)	N (18, 2.5)
EVCS-5 and EVCS-6	N (9, 2.5)	N (17, 2.5)

Note: In $N(\mu, \sigma)$, μ and σ represent the mean time (24-h format) and standard deviation (h), respectively.

3.2. Study Scenarios

The proposed scheduling framework is examined under deterministic as well as uncertainty-aware operating conditions. A deterministic operating point is first obtained

using forecasted load demand and renewable generation data. The resulting deterministic operating cost is then adopted as the reference value for estimating the admissible uncertainty radius within the risk-averse IGDT framework. The study scenarios investigated are summarized in Table 6.

Table 6. Uncertainty representation across different scenarios.

Uncertainty Source	Scenario 1	Scenario 2	Scenario 3	Scenario 4
Load Demand	Deterministic	Uncertain	Deterministic	Uncertain
Renewable Generation	Deterministic	Deterministic	Uncertain	Uncertain

3.2.1. Scenario 1

Scenario 1 represents the deterministic operating condition in which forecasted load demand and renewable generation are assumed to be perfectly known, and no uncertainty is considered. The external grid active power profile for Scenario 1 is presented in Figure 6. The grid active power import follows the hourly electricity tariff variation. Higher grid imports are observed during low and moderate electricity price intervals, whereas comparatively lower imports occur during expensive operating periods. The reduced grid requirement during evening hours is mainly due to DG support and BESS discharging through ESOP operation. According to the active energy balance results in Table 7, the total grid energy imported under Scenario 1 is 35,299.52 kWh.

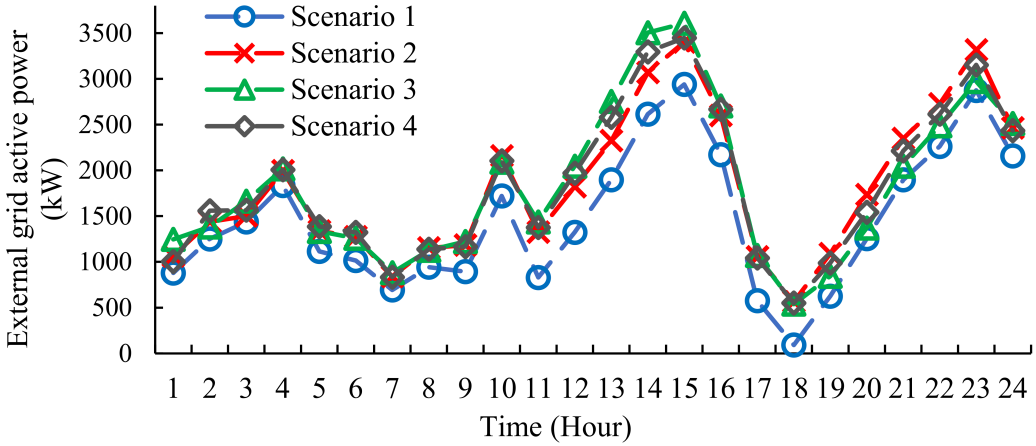


Figure 6. External grid active power under different scenarios.

Table 7. Active energy balance under different study scenarios (kWh).

Scenario	Grid Energy	DEG Energy	Solar Energy	Wind Energy	ESOP Losses	Line Losses	Aggregate Load Energy Consumption	Energy Consumption of All EVCSs
1	35,299.52	3017.44	13,511.68	12,905.63	472.99	651.08	54,954.26	8655.93
2	43,787.82	3056.79	13,490.69	12,896.84	525.35	867.52	63,189.02	8650.24
3	44,117.51	3060.76	8963.51	8579.08	439.74	832.49	54,790.03	8658.61
4	43,962.32	3056.41	11,214.89	10,722.25	465.74	843.57	58,986.50	8660.06

Note: Scenarios 2–4 correspond to $\sigma = 0.2$. Scenario 4 represents a representative operating point selected from feasible load–renewable uncertainty combinations under fixed operating budget.

The DG active power scheduling profile shown in Figure 7 indicates that the DG unit remains inactive during low-cost periods and operates only during hours 17–21, which correspond to high grid power cost intervals. The DG output reaches a maximum value of 690.49 kW at hour 19. Such operation reduces dependence on expensive grid energy

during peak demand periods and improves the operating economy of the ADN. The total DG energy contribution under Scenario 1 is 3017.44 kWh.

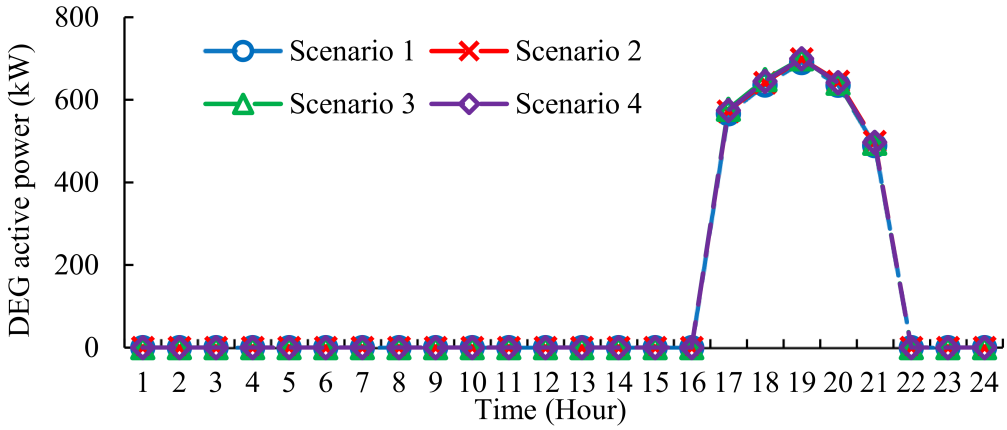


Figure 7. DG active power under different scenarios.

The optimized load profile after DSM implementation is compared with the pre-DSM load profile in Figure 8. The DSM strategy shifts a portion of the load toward lower electricity price intervals while reducing demand during high-cost operating periods. Demand shifting toward low-cost intervals is mainly observed during hours 1–8, whereas demand reduction is noticeable during hours 17–22. This coordinated demand adjustment improves load distribution over the scheduling horizon and reduces stress during peak-price periods. The total aggregate load energy consumption under Scenario 1 is 54,954.26 kWh, while the corresponding reactive energy demand is 32,041.60 kVARh.

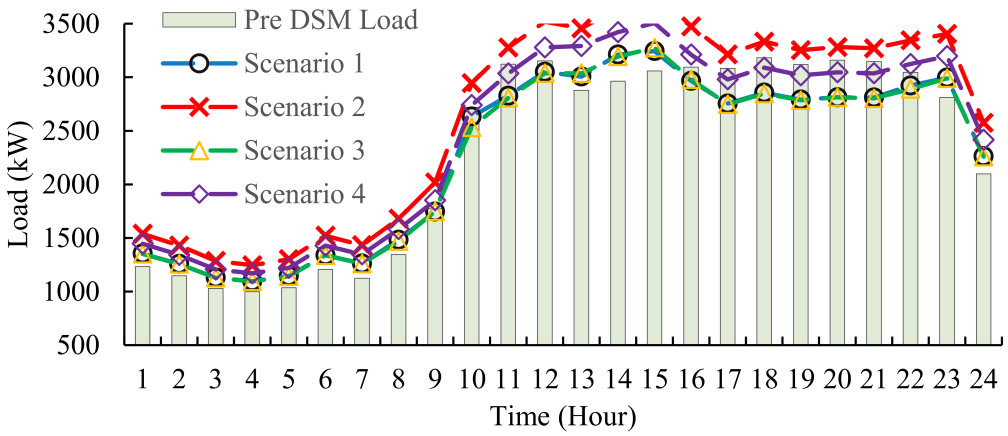


Figure 8. Load profile under different scenarios.

The ESOP scheduling characteristics for Scenario 1 are illustrated in Figures 9 and 10. The 24-h operating schedules of the two ESOPs demonstrate bidirectional active power exchange between interconnected feeders together with coordinated charging and discharging operation of the embedded BESS units. ESOP power transfer and BESS scheduling are primarily governed by the hourly electricity price. Accordingly, the batteries charge during lower-price intervals and discharge during higher-price operating periods. When the BESS remains idle, direct feeder-to-feeder power transfer occurs through the ESOP terminals, indicating the additional role of ESOP in feeder power balancing. Positive charging power is mainly observed during hours 3–5 and hour 14, whereas battery discharging occurs during hours 11 and 18–20. The SOC profile follows the charging and discharging pattern appropriately, increasing close to 1 p.u. during charging intervals and decreasing to nearly

0.2 p.u. during peak support periods. At the end of the scheduling horizon, the SOC returns to 0.4 p.u., thereby satisfying cyclic battery operating constraints.

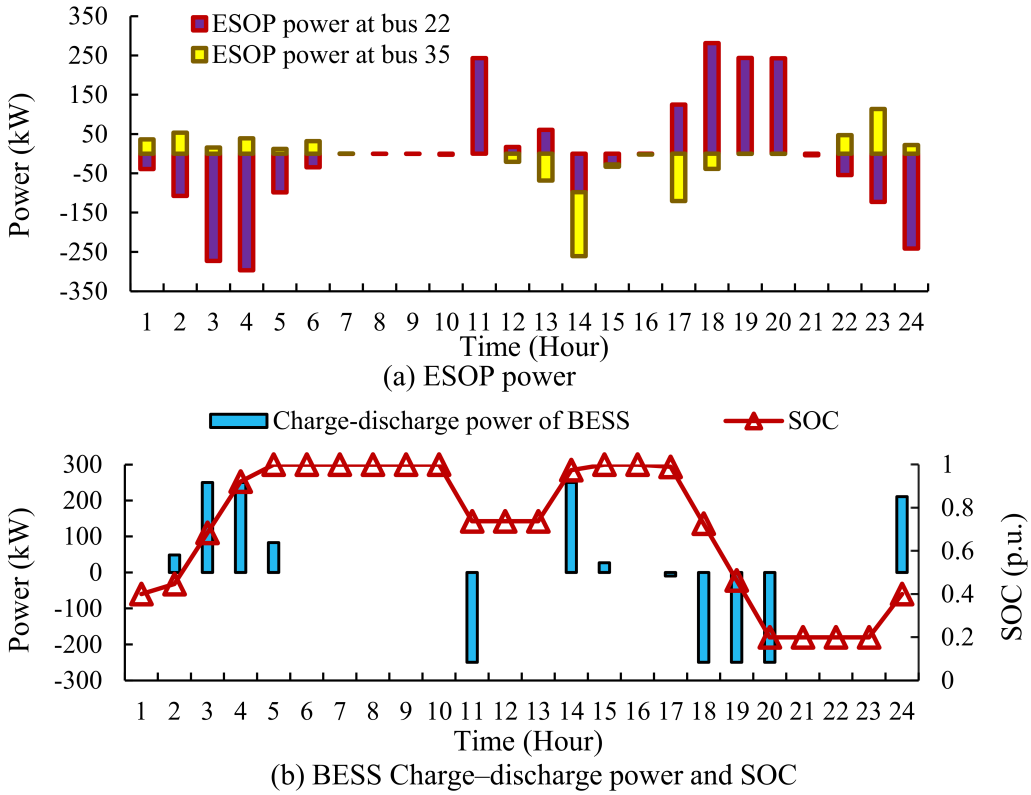


Figure 9. ESOP 1 scheduling under Scenario 1.

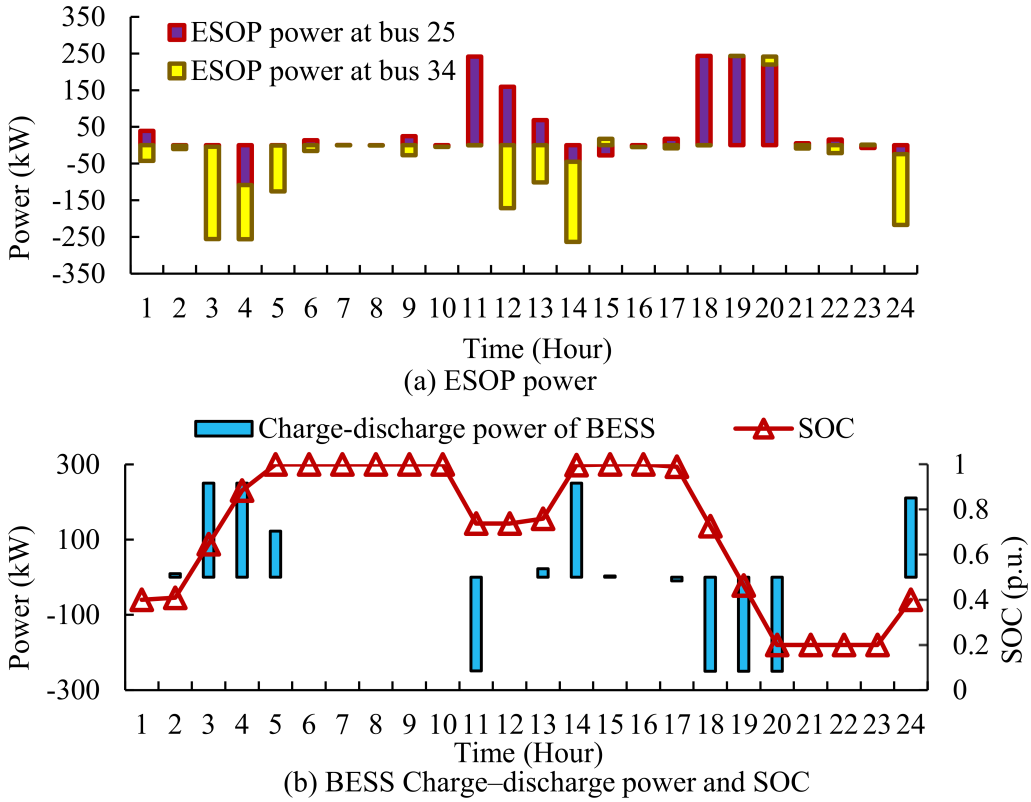


Figure 10. ESOP 2 scheduling under Scenario 1.

The active energy balance results summarized in Table 7 indicate a significant contribution from renewable energy resources toward meeting the system demand. Under Scenario 1, the PV and wind generation systems supply 13,511.68 kWh and 12,905.63 kWh, respectively, while the DG contributes 3017.44 kWh. The ESOP converter losses and network line losses are limited to 472.99 kWh and 651.08 kWh, respectively, indicating efficient network operation. The total EVCS charging demand under Scenario 1 is 8655.93 kWh.

The reactive power scheduling under Scenario 1 is shown in Figure 11. The reactive energy balance results presented in Table 8 indicate that the reactive power requirement of the ADN is predominantly supplied by local resources. The reactive energy contribution from the external grid remains zero, confirming adequate reactive support from DGs, renewable generators, and ESOP converters. PV systems contribute 9924.90 kVARh, wind generators supply 8191.71 kVARh, and ESOP converters inject 10,054.26 kVARh of reactive energy support.

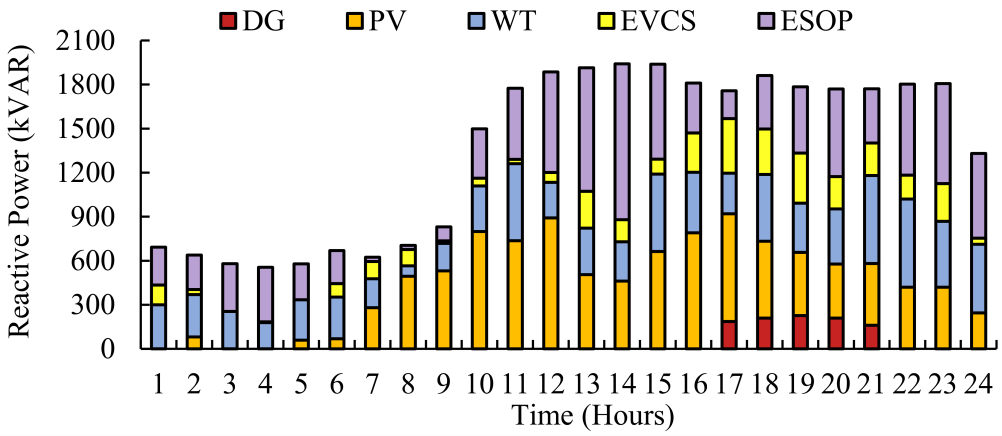


Figure 11. Reactive power scheduling under Scenario 1.

Table 8. Reactive energy balance under different study scenarios (kVARh).

Scenario	Grid Reactive Energy	DEG Reactive Energy	Reactive Energy from PV	Reactive Energy from WT	Line Reactive Energy Losses	Reactive Energy from ESOP	Reactive Energy Demand of the Load	Reactive Energy from EVCSs
1	0.00	991.78	9924.90	8191.71	477.98	10,054.26	32,041.60	3356.92
2	90.47	1004.72	11,213.21	8741.23	626.43	12,749.05	36,404.52	3232.29
3	4.16	1006.02	10,325.91	7787.62	588.01	9099.89	31,501.65	3866.06
4	0.00	1004.20	11,119.04	8801.03	603.26	10,087.28	33,951.47	3543.19

Note: Same study conditions as Table 7.

The aggregated EVCS power scheduling profiles for Scenario 1 are presented in Figure 12. The EVCS aggregated power profiles follow coordinated economic charging behavior according to electricity price variation and system operating conditions. Higher EV charging demand is mainly scheduled during lower-price intervals, whereas reduced charging or V2G support is observed during expensive operating periods. This coordinated EV scheduling assists in peak reduction and improves operational flexibility of the ADN.

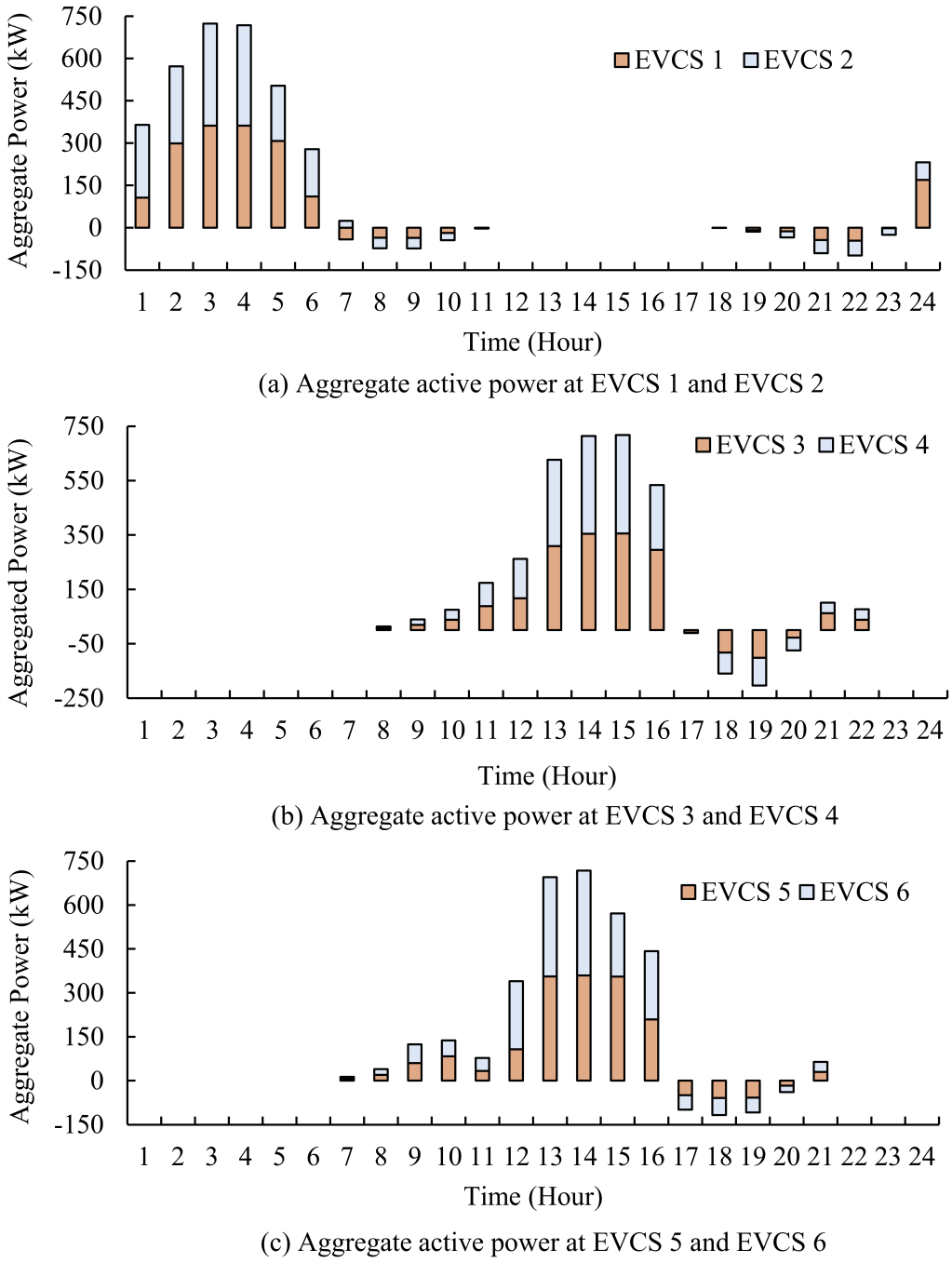


Figure 12. Aggregated EVCS active power scheduling under Scenario 1.

3.2.2. Scenario 2

Scenario 2 investigates the effect of load-demand uncertainty while renewable generation remains deterministic. The allowable operating budget is progressively relaxed with respect to the deterministic operating cost using the deviation factors of 0.05 p.u., 0.10 p.u., 0.15 p.u., and 0.20 p.u. The corresponding variation of admissible load uncertainty with deviation factor is illustrated in Figure 13. It is observed that the admissible load uncertainty increases steadily with the permissible budget relaxation and reaches 15.30% at a deviation factor of 0.20 p.u. The operating characteristics corresponding to the deviation factor of 0.20 p.u. are considered for detailed comparison with the deterministic operating condition of Scenario 1.

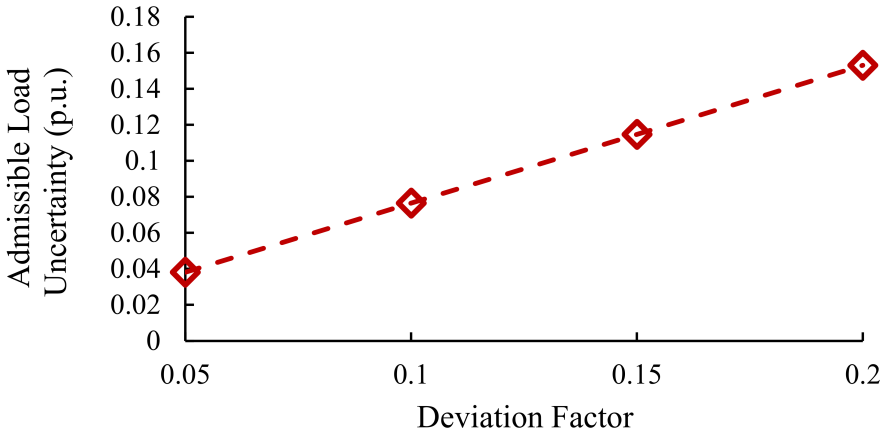


Figure 13. Effect of deviation factor on admissible load uncertainty.

The load-demand profile under Scenario 2 remains consistently higher than that of Scenario 1, as shown in Figure 8. Owing to the increase in demand, the active power imported from the utility grid also rises noticeably, whereas the DG scheduling pattern remains nearly unchanged. The DG contribution therefore exhibits only marginal variation, indicating that the additional demand requirement is primarily accommodated through increased grid power import rather than substantial rescheduling of local generation resources.

The active energy balance summarized in Table 7 further supports this behavior. Under Scenario 2, the total load energy demand increases from 54,954.26 kWh in Scenario 1 to 63,189.02 kWh, while line losses rise from 651.08 kWh to 867.52 kWh. Correspondingly, grid energy import increases significantly from 35,299.52 kWh to 43,787.82 kWh, confirming that the increased demand and associated network losses are predominantly supplied through the external grid. In contrast, DG energy contribution changes only marginally from 3017.44 kWh to 3056.79 kWh. The renewable energy contribution exhibits a slight reduction compared with the deterministic condition, where solar energy decreases from 13,511.68 kWh to 13,490.69 kWh and wind energy decreases from 12,905.63 kWh to 12,896.84 kWh. This behavior is mainly associated with the enhanced reactive power support provided by inverter-based renewable sources under higher load-demand conditions.

The reactive power scheduling profile corresponding to Scenario 2 is shown in Figure 14. Compared with Scenario 1, the net reactive power profile remains at a comparatively higher level during most operating intervals owing to the increase in load-driven reactive power demand. The reactive energy balance presented in Table 8 indicates that the total reactive energy demand of the load increases from 32,041.60 kVARh to 36,404.52 kVARh, while reactive energy losses also increase from 477.98 kVARh to 626.43 kVARh. To satisfy this additional reactive requirement, the reactive energy support from PV and WT units increases noticeably. The reactive energy supplied by PV units rises from 9924.90 kVARh to 11,213.21 kVARh, while the WT contribution increases from 8191.71 kVARh to 8741.23 kVARh. Similarly, reactive energy support from the ESOP increases from 10,054.26 kVARh to 12,749.05 kVARh. The increased reactive power participation of renewable sources explains the marginal reduction observed in their active energy contribution under Scenario 2.

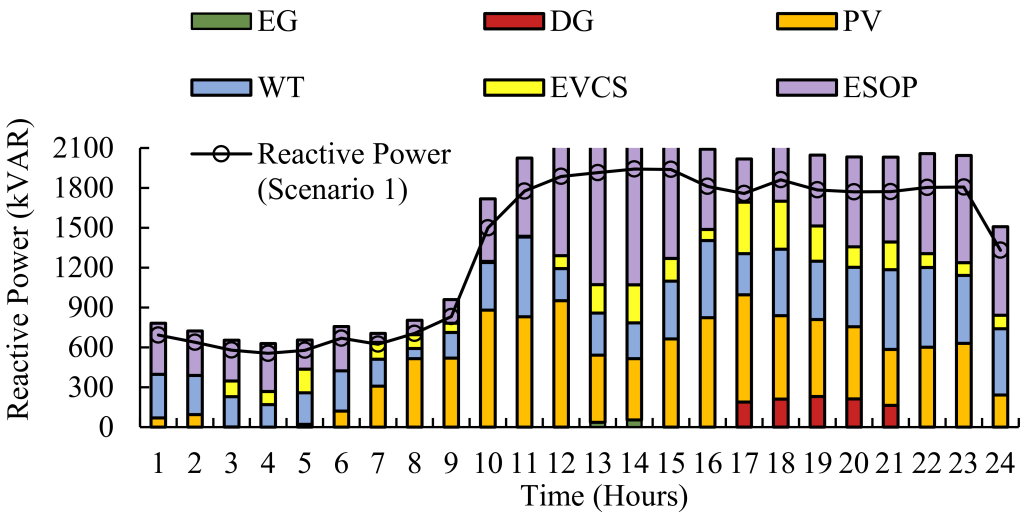


Figure 14. Reactive power scheduling under Scenario 2.

The ESOP scheduling behavior under load uncertainty remains broadly similar to that observed under deterministic operation; therefore, a separate ESOP scheduling profile is not presented for this scenario. Likewise, the aggregate EVPL scheduling pattern exhibits only negligible variation relative to Scenario 1. This behavior is mainly attributed to the fact that EV charging and discharging decisions are strongly influenced by the hourly grid electricity price within the permissible arrival and departure constraints. Consequently, EVs continue to charge predominantly during lower-price periods, while only limited discharging occurs during higher-price intervals, resulting in nearly similar scheduling behavior across different study scenarios.

As indicated in Table 9, the ADN operating cost increases from \$5230.04 in Scenario 1 to \$6276.07 under load-uncertainty conditions. This increase is primarily governed by the higher cost associated with utility-grid energy procurement, which rises from \$3931.24 to \$4970.98 owing to the substantial increase in grid energy import. In contrast, the operating cost contributions associated with DG generation, DSM operation, and EV charging remain nearly unchanged. This observation further confirms that the principal impact of load uncertainty is reflected through increased dependence on external grid support to satisfy the additional demand and associated network losses.

Table 9. Operating cost decomposition under different study scenarios (\$).

Scenario	Cost of Energy from EG	Cost of Reactive Energy from EG	Cost of Energy from DEG	Cost of Reactive Energy from DEG	Cost of DSM	Total EV Charging Cost Across All EVCSs	ADN Operating Cost
1	3931.236	0	412.027	0.41	18.388	868	5230.043
2	4970.977	0.507	417.818	0.41	18.351	868.01	6276.072
3	4970.806	0.024	418.307	0.41	18.375	868.15	6276.072
4	4971.22	0	417.603	0.41	18.654	868.185	6276.072

Note: Same study conditions as Table 7.

3.2.3. Scenario 3

Scenario 3 investigates the effect of renewable-generation uncertainty while maintaining deterministic load demand. Similar to Scenario 2, the allowable operating budget is progressively relaxed with respect to the deterministic operating cost using deviation factors of 0.05 p.u., 0.10 p.u., 0.15 p.u., and 0.20 p.u. The corresponding variation of admissible renewable uncertainty with a deviation factor is illustrated in Figure 15. It is observed that

the admissible renewable uncertainty increases consistently with the permissible budget relaxation and reaches 0.33306 p.u. at a deviation factor of 0.20 p.u. The operating characteristics corresponding to the deviation factor of 0.20 p.u. are considered for detailed comparison with the deterministic operating condition of Scenario 1.

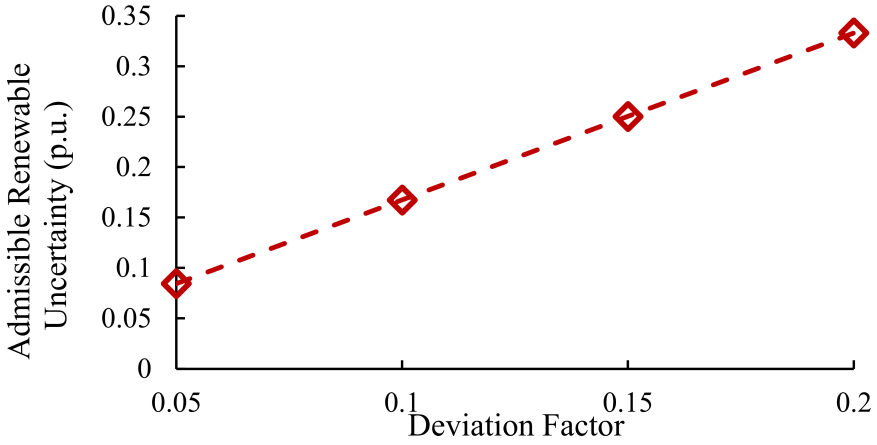


Figure 15. Effect of deviation factor on admissible renewable uncertainty.

The load-demand profile under Scenario 3 remains nearly identical to that observed under deterministic operation, as shown in Figure 8, since uncertainty is considered only for renewable generation while the load demand remains unchanged. Similarly, the DG scheduling profile exhibits only marginal variation relative to Scenario 1. However, owing to the reduction in available renewable power under uncertainty conditions, the active power imported from the external grid increases noticeably, as illustrated in Figure 6. This behavior indicates that the reduction in renewable generation is primarily compensated through additional grid power import rather than substantial rescheduling of the DG output.

The active energy balance summarized in Table 7 further supports this operational behavior. Under Scenario 3, the solar-energy contribution decreases significantly from 13,511.68 kWh in Scenario 1 to 8963.51 kWh, while the wind-energy contribution decreases from 12,905.63 kWh to 8579.08 kWh owing to renewable uncertainty. Correspondingly, grid energy import increases substantially from 35,299.52 kWh to 44,117.51 kWh. In contrast, DG generation changes only marginally from 3017.44 kWh to 3060.76 kWh. Since the load demand remains nearly unchanged relative to Scenario 1, the increase in grid import primarily compensates for the reduction in renewable energy contribution and the associated increase in network losses. Line losses increase from 651.08 kWh to 832.49 kWh under renewable uncertainty conditions, further contributing to the increased grid-energy requirement.

The reactive energy balance corresponding to Scenario 3 is presented in Table 8, while the hourly reactive power scheduling profile is shown in Figure 16. Compared with Scenario 1, the reactive energy demand of the load remains comparatively close because the load profile remains deterministic. However, variations in renewable power availability influence the reactive power contribution from inverter-based renewable units and associated reactive power exchange within the network. The reactive energy supplied by PV units increases from 9924.90 kVARh in Scenario 1 to 10,325.91 kVARh under renewable uncertainty conditions, while the WT reactive energy contribution slightly decreases from 8191.71 kVARh to 7787.62 kVARh. Reactive energy support from the ESOP remains significant, contributing 9099.89 kVARh to maintaining reactive power balance and voltage support across the network. Reactive energy losses also increase from

477.98 kVARh to 588.01 kVARh owing to the modified power-flow conditions under reduced renewable generation.

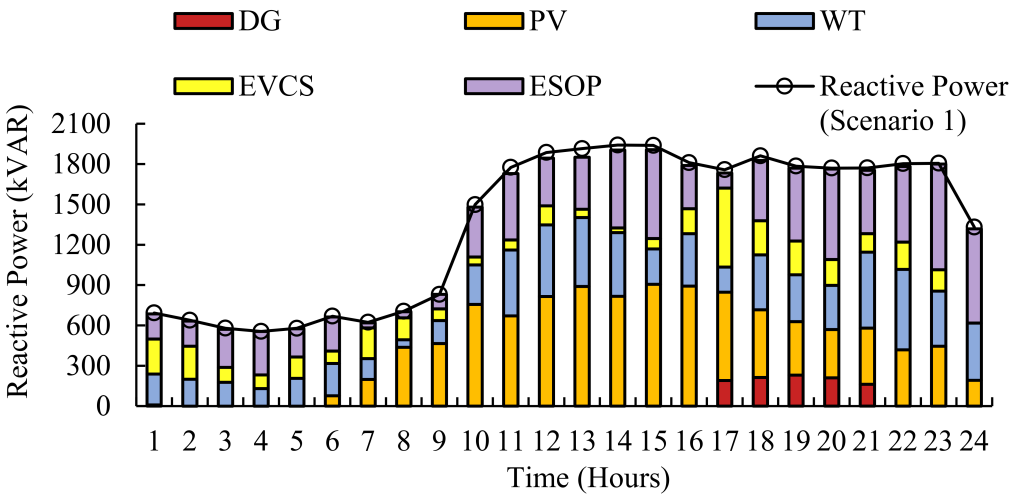


Figure 16. Reactive power scheduling under Scenario 3.

The ESOP scheduling behavior under renewable uncertainty remains broadly similar to that observed under deterministic operation and load-uncertainty conditions; therefore, separate ESOP scheduling curves are not presented for this scenario. Likewise, the aggregate EVCS scheduling behavior exhibits only negligible variation relative to Scenarios 1 and 2.

As indicated in Table 9, compared with Scenario 1, the ADN operating cost increases from \$5230.04 (Scenario 1) to \$6276.07 under renewable uncertainty conditions. This increase is primarily associated with the higher cost of grid-energy procurement, which rises from \$3931.24 (Scenario 1) to \$4970.81 due to the substantial increase in external grid power import required to compensate for reduced renewable generation. In contrast, the operating costs associated with DG scheduling, DSM operation, and EV charging remain nearly unchanged. These results indicate that renewable-generation uncertainty predominantly affects system operation through increased dependence on utility-grid support to maintain power balance and satisfy network demand.

3.2.4. Scenario 4

Scenario 4 examines the simultaneous impact of load-demand and renewable-generation uncertainty within the proposed risk-averse IGDT framework. In this case, the allowable operating cost is fixed at 1.2 times the deterministic operating cost, corresponding to a deviation factor of 0.20 p.u. The analysis begins from the maximum admissible load uncertainty obtained under Scenario 2, following which the load uncertainty level is progressively reduced in steps of 10% of the maximum admissible load uncertainty. For each specified load-uncertainty level, the admissible renewable uncertainty is maximized to determine feasible uncertainty combinations under the fixed operating budget. The resulting variation between admissible load and renewable uncertainty is illustrated in Figure 17.

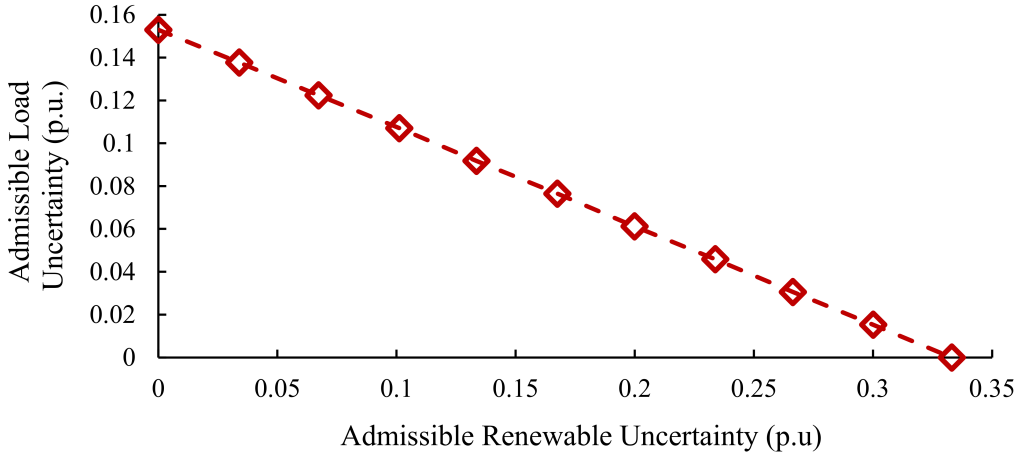


Figure 17. Load–renewable uncertainty variation under fixed operating budget.

To facilitate comparative operational analysis with the previous study scenarios, a representative operating point corresponding to load uncertainty of 0.0765 p.u. and renewable uncertainty of 0.1674 p.u. is selected from the uncertainty variation characteristics shown in Figure 17. The operating behavior corresponding to this representative uncertainty combination is subsequently compared with the deterministic operating condition of Scenario 1.

Since Scenario 4 simultaneously incorporates increased load demand and reduced renewable availability, the resulting load profile remains generally between the profiles obtained under Scenarios 1 and 2, as shown in Figure 8. Similarly, the reduction in renewable generation together with the increase in demand leads to higher dependence on utility-grid support. Consequently, the grid active power profile remains consistently above the deterministic profile during most operating intervals, whereas the DG scheduling pattern exhibits only marginal variation compared with the previous study scenarios.

The active energy balance summarized in Table 7 further supports these observations. Under Scenario 4, aggregate load energy consumption increases from 54,954.26 kWh in Scenario 1 to 58,986.50 kWh, while line losses increase from 651.08 kWh to 843.57 kWh. At the same time, renewable energy contribution decreases relative to deterministic operation, where solar energy decreases from 13,511.68 kWh to 11,214.89 kWh and wind energy decreases from 12,905.63 kWh to 10,722.25 kWh. To compensate for the combined effect of increased demand, reduced renewable generation, and additional network losses, grid energy import increases significantly from 35,299.52 kWh to 43,962.32 kWh. In contrast, DG energy contribution changes only marginally from 3017.44 kWh to 3056.41 kWh, indicating that the primary operational adjustment under combined uncertainty conditions is achieved through increased external-grid support.

The reactive power scheduling profile corresponding to Scenario 4 is shown in Figure 18. The reactive energy balance presented in Table 8 indicates that the total reactive energy demand of the load increases from 32,041.60 kVARh in Scenario 1 to 33,951.47 kVARh under combined uncertainty conditions. Similarly, reactive energy losses increase from 477.98 kVARh to 603.26 kVARh due to modified network operating conditions. To maintain reactive power balance and voltage support within the distribution network, inverter-based renewable sources and ESOP units provide substantial reactive energy support. The reactive energy supplied by PV units increases from 9924.90 kVARh to 11,119.04 kVARh, while WT reactive energy contribution increases from 8191.71 kVARh to 8801.03 kVARh. Reactive energy support from the ESOP remains significant at 10,087.28 kVARh, thereby contributing to reactive power compensation and network voltage regulation under simultaneous uncertainty conditions. The ESOP and EVCS scheduling characteristics under Scenario

4 remain broadly similar to those observed under the previous operating scenarios and therefore are not presented separately.

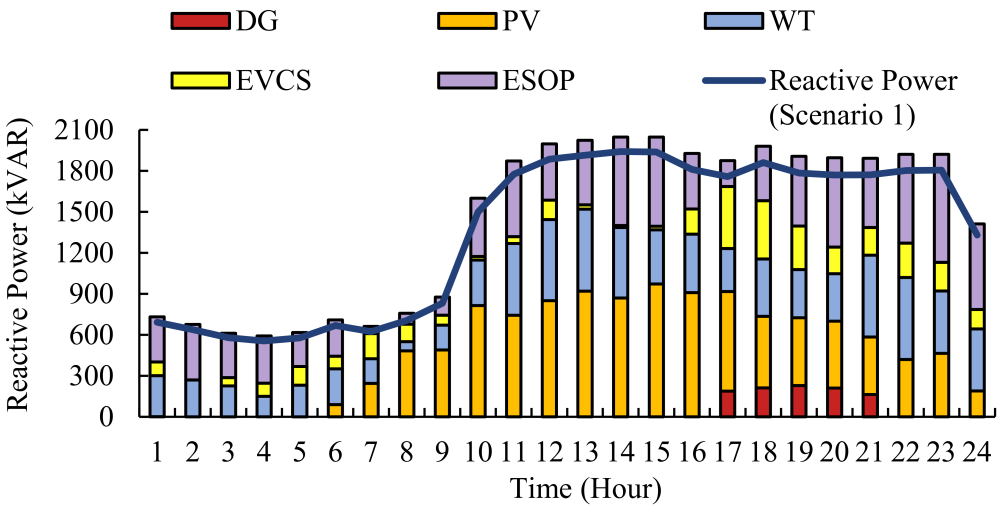


Figure 18. Reactive power scheduling under Scenario 4.

The operating cost decomposition corresponding to Scenario 4 is summarized in Table 9. Compared with the deterministic operating condition, the ADN operating cost increases from \$5230.04 to \$6276.26 under simultaneous load and renewable uncertainty. Similar to the previous uncertainty scenarios, the dominant contribution to the increased operating expenditure arises from the higher cost associated with external-grid energy procurement, which increases from \$3931.24 to \$4971.22 owing to the substantial rise in grid energy import. In contrast, the cost components associated with DG operation, DSM participation, and EV charging remain nearly unchanged. These results indicate that the combined effect of load and renewable uncertainty is primarily reflected through increased dependence on utility-grid support to maintain power balance and satisfy network demand under constrained operating conditions.

3.2.5. Sensitivity Analysis of Admissible Load and Renewable Uncertainty Limits Under Variations in Electricity Price, EV Participation, Demand-Side Flexibility, and ESOP Size

The representative uncertainty point considered in this sensitivity analysis is selected from the load–renewable uncertainty variation frontier established for Scenario 4. At this operating point, the admissible load and renewable uncertainty limits are 0.0765 p.u. and 0.1674 p.u., respectively, while satisfying the prescribed economic-performance requirement. To further examine the factors influencing uncertainty accommodation capability, additional sensitivity studies are performed by varying electricity price, demand-side management (DSM) participation, EV participation levels, and ESOP size. In each case, only one parameter is modified while all remaining model parameters are maintained unchanged. Admissible renewable uncertainty is evaluated by fixing the load-uncertainty radius at its representative value, whereas admissible load uncertainty is determined by fixing the renewable-uncertainty radius at its representative value. The corresponding sensitivity-analysis results are summarized in Table 10.

Table 10. Sensitivity analysis of admissible load and renewable uncertainty limits under variations in electricity price, EV participation, and demand-side flexibility.

Parameter	Case	Admissible α^R (p.u.)	Admissible α^L (p.u.)
Electricity Price	5% decrease in grid energy price	0.251	0.115
	5% increase in grid energy price	0.090	0.041
DSM Participation	10% DSM participation	0.155	0.071
	30% DSM participation	0.179	0.082
EV Participation	25 EVs/EVCS (150 EVs total)	0.274	0.126
	35 EVs/EVCS (210 EVs total)	0.094	0.043
ESOP (SOP with BESS)	SOP Converter 400 kVA, BESS capacity 800 kWh (charge/discharge limit 200 kW)	0.157	0.074
	Converter 600 kVA, BESS capacity 1200 kWh (charge discharge limit 300 kW)	0.173	0.079

The results indicate that electricity price has a pronounced influence on admissible uncertainty limits. A 5% reduction in grid energy price increases the admissible renewable uncertainty from 0.1674 p.u. to 0.251 p.u. and the admissible load uncertainty from 0.0765 p.u. to 0.115 p.u. In contrast, a 5% increase in electricity price reduces the corresponding uncertainty limits to 0.090 p.u. and 0.041 p.u., respectively. This behavior is expected because lower energy procurement costs provide additional economic headroom within the IGDT performance requirement, whereas higher electricity prices accelerate the exhaustion of the allowable operating-cost margin.

DSM participation exhibits a comparatively moderate but beneficial effect on uncertainty accommodation capability. Reducing DSM participation from the reference level of 20% to 10% decreases the admissible renewable and load uncertainty limits to 0.155 p.u. and 0.071 p.u., respectively. Conversely, increasing DSM participation to 30% raises the admissible renewable uncertainty to 0.179 p.u. and the admissible load uncertainty to 0.082 p.u. The improvement can be attributed to the enhanced load-shifting capability available under higher DSM participation, which provides additional operational flexibility for balancing uncertain operating conditions.

The influence of EV participation is more pronounced. For the investigated operating conditions, reducing the number of EVs from 180 to 150 increases the admissible renewable and load uncertainty limits to 0.274 p.u. and 0.126 p.u., respectively. In contrast, increasing the EV population to 210 reduces the corresponding admissible uncertainty limits to 0.094 p.u. and 0.043 p.u. This trend indicates that, under the adopted charging and scheduling assumptions, the additional charging demand associated with higher EV penetration outweighs the flexibility benefits provided by EV participation, thereby reducing the uncertainty accommodation capability available within the prescribed economic-performance requirement.

The influence of ESOP sizing on uncertainty accommodation is also investigated by varying the SOP converter rating and the associated BESS capacity from the reference configuration of a 500 kVA converter with a 1000 kWh battery (250 kW charge/discharge

limit). Reducing the ESOP size to a 400 kVA converter with an 800 kWh battery (200 kW charge/discharge limit) decreases the admissible renewable uncertainty from 0.1674 p.u. to 0.157 p.u. and the admissible load uncertainty from 0.0765 p.u. to 0.074 p.u. Conversely, increasing the ESOP capacity to a 600 kVA converter with a 1200 kWh battery (300 kW charge/discharge limit) increases the admissible renewable and load uncertainty limits to 0.173 p.u. and 0.079 p.u., respectively. The increase in admissible uncertainty is relatively modest because the reference ESOP configuration already provides sufficient operational flexibility at the selected representative operating point. Under these conditions, further increases in the converter rating and battery capacity offer only limited additional flexibility for uncertainty accommodation. Nevertheless, the consistent improvement observed in both admissible renewable and load uncertainty limits indicates that larger ESOP capacities can further strengthen the network's capability to operate within the prescribed economic-performance requirement under uncertain operating conditions.

In a nutshell, the sensitivity analysis demonstrates that the admissible uncertainty limits obtained through the IGDT framework are strongly influenced by economic and operational flexibility factors. Lower electricity prices and increased DSM participation improve uncertainty accommodation capability, whereas the impact of EV participation depends on the balance between the flexibility services provided by EVs and the additional charging demand imposed on the distribution network. The ESOP sizing results further indicate that larger converter and battery capacities support slightly higher admissible renewable and load uncertainty limits under the prescribed economic-performance requirement.

The proposed optimization framework is implemented in GAMS 41.3 and solved using the DICOPT solver, with CONOPT and CPLEX employed to handle the NLP and MIP subproblems, respectively. All simulations are carried out on a workstation equipped with an Intel Core i7-12700F processor operating at 2.10 GHz and 16 GB of RAM. Across all investigated operating conditions, the average computational time is 1371 s. The solution procedure terminates normally and returns the best integer-feasible solution identified by the solver. All investigated scenarios and sensitivity studies converge successfully and produce feasible operating schedules without encountering infeasible operating conditions.

4. Conclusions & Future Scope

A risk-averse IGDT-based scheduling approach for coordinated active and reactive power management in an active distribution network has been presented in this work. The proposed framework integrates renewable energy sources, diesel generation, demand-side management, electric vehicle parking lots, and energy-storage-assisted soft open points within a modified IEEE 33-bus distribution system. The scheduling problem was formulated by considering network operating constraints, voltage-sensitive load behavior, and coordinated active–reactive power dispatch under uncertain operating conditions. Initially, a deterministic operating condition was established as the reference case, following which the influence of load-demand and renewable-generation uncertainty was examined through the IGDT methodology.

The results obtained indicate that the admissible uncertainty level increases with permissible operating-budget relaxation under both load and renewable uncertainty conditions. Under load uncertainty, the additional demand and associated network losses were mainly compensated through increased utility-grid power import, while local DG scheduling exhibited comparatively small variation. In the case of renewable uncertainty, the reduction in renewable energy availability similarly increased dependence on external-grid support for maintaining system power balance. Furthermore, simultaneous consideration of load and renewable uncertainty enabled the identification of feasible uncertainty com-

binations under a fixed operating budget, thereby illustrating the operational interaction between admissible load and renewable uncertainty levels.

The study also demonstrated the significant contribution of inverter-based renewable units and ESOPs toward reactive power support and voltage regulation during uncertain operating conditions. Although uncertainty affected total power exchange and operating expenditure, the scheduling behavior of ESOPs and EV parking lots remained comparatively consistent across the investigated operating scenarios. The operating cost analysis revealed that the principal variation in ADN operating cost was predominantly associated with increased grid-energy procurement under uncertainty conditions. The proposed framework therefore provides an effective approach for uncertainty-aware coordinated scheduling while maintaining operational feasibility and network security within the specified risk budget.

Future research may explore the application of the proposed framework to larger and more complex distribution systems by employing convex reformulation strategies and distributed solution methodologies. Such enhancements would improve computational efficiency and scalability, enabling practical deployment in converter-intensive and hybrid AC/DC distribution networks. Another promising research direction involves the incorporation of advanced battery-energy-storage management schemes, including distributed state-of-charge coordination, cooperative power-sharing mechanisms, and multi-agent control architectures, to further improve the operational effectiveness of storage resources [33,34]. Integrating such real-time battery-management capabilities with day-ahead scheduling and uncertainty-aware operational planning offers an interesting avenue for future research.

Moreover, future studies may also investigate alternative approaches for representing uncertainty associated with renewable generation, demand variability, electric-vehicle participation, and electricity-market conditions. The adoption of stochastic, robust, distributionally robust, and chance-constrained optimization frameworks could provide additional perspectives on balancing economic objectives with secure system operation under uncertain environments.

Author Contributions: Conceptualization, S.P.S.; methodology, S.P.S. and N.K.; software, S.P.S.; validation, S.P.S. and N.K.; formal analysis, S.P.S.; investigation, S.P.S. and N.K.; resources, N.K. and A.S.; data curation, S.P.S.; writing—original draft preparation, S.P.S.; writing—review and editing, N.K., A.S. and V.R.; visualization, N.K., A.S. and V.R.; supervision, N.K. and A.S.; project administration, N.K. and V.R.; funding acquisition, V.R. All authors have read and agreed to the published version of the manuscript.

Funding: This research received no external funding.

Data Availability Statement: Data sets generated during the current study are available from the first author on reasonable request.

Acknowledgments: The authors gratefully acknowledge the use of computing facilities at the Power System Laboratory of Electrical Engineering Department, Manipal University Jaipur, for supporting the research activities.

Conflicts of Interest: The authors declare no conflicts of interest.

References

1. Sharma, S.; Niazi, K.R.; Verma, K.; Rawat, T. Coordination of different DGs, BESS and demand response for multi-objective optimization of distribution network with special reference to Indian power sector. *Int. J. Electr. Power Energy Syst.* **2020**, *121*, 106074. [CrossRef]
2. Rawat, T.; Niazi, K.R.; Gupta, N.; Sharma, S. Multi-objective techno-economic operation of smart distribution network integrated with reactive power support of battery storage systems. *Sustain. Cities Soc.* **2021**, *75*, 103359.

3. Gangil, G.; Goyal, S.K.; Saraswat, A. A multi-objective techno-economic operation of distribution network considering reactive power support from renewable energy and battery storage system. *J. Energy Storage* **2024**, *102*, 114116.
4. Wang, J.; Wang, W.Q.; Wang, H.Y. Bi-stage operation optimization of active distribution networks with soft open point considering violation risk. *Energy Rep.* **2022**, *8*, 14947–14961. [CrossRef]
5. Wang, J.; Zhou, N.; Tao, A.; Wang, Q. Optimal operation of soft open points-based energy storage in active distribution networks by considering battery lifetime. *Front. Energy Res.* **2021**, *8*, 633401.
6. Gholami, K.; Azizivahed, A.; Arefi, A.; Rahman, M.M.; Islam, M.R.; Li, L.; Arif, M.T.; Haque, M.E. Hybrid uncertainty approach for management of energy storage-embedded soft open points in distribution grids. *J. Energy Storage* **2024**, *87*, 111394. [CrossRef]
7. Vijayan, V.; Arzani, A.; Mahajan, S.M. Demand side management considering load–voltage interdependence and optimal topology selection in active distribution networks. *IEEE Access* **2025**, *13*, 49107–49120. [CrossRef]
8. Saxena, V.; Rajput, S.K.; Manna, S.; Gantayet, A.; Agarwal, K.L.; Alsharif, M.H.; Kim, M.-K. Bi-level optimization for demand response integration with solar PV and battery energy storage systems. *Energy Rep.* **2026**, *15*, 108882.
9. Chadha, S.; Jain, V.; Chandna, V.K. Hybrid optimization algorithm based demand side management and energy scheduling in EV charging station. *J. Energy Storage* **2026**, *151*, 120076. [CrossRef]
10. Pamshetti, V.B.; Singh, S.; Thakur, A.K.; Singh, S.P. Multistage coordination Volt/VAR control with CVR in active distribution network in presence of inverter-based DG units and soft open points. *IEEE Trans. Ind. Appl.* **2021**, *57*, 2035–2047.
11. Pamshetti, V.B.; Singh, S.; Thakur, A.K.; Singh, S.P.; Babu, T.S.; Patnaik, N.; Krishna, G.H. Cooperative operational planning model for distributed energy resources with soft open point in active distribution network. *IEEE Trans. Ind. Appl.* **2022**, *59*, 2140–2151. [CrossRef]
12. Singh, S.P.; Kanwar, N.; Saraswat, A. Optimal operation of active distribution network considering energy storage-equipped soft open points. *e-Prime* **2025**, *13*, 101082.
13. Arias, A.; Granada, M.; Castro, C.A. Optimal probabilistic charging of electric vehicles in distribution systems. *IET Electr. Syst. Transp.* **2017**, *7*, 246–251. [CrossRef]
14. Kashki, A.; Azarfar, A.; Moghaddam, M.S.; Davarzani, R. Optimal charging of electric vehicles in smart stations and its effects on the distribution network using meerkat optimization algorithm. *Energy Rep.* **2024**, *12*, 1936–1946. [CrossRef]
15. Tavalaei, H.; Moghaddam, M.S.; Vahedi, M.; Salehi, N.; Abardeh, M.H. Energy management in smart distribution networks: Synergizing network reconfiguration, energy storage, and electric vehicles with disjunctive convex hull relaxation. *Energy Rep.* **2024**, *12*, 5999–6015. [CrossRef]
16. Pirouzi, S.; Latify, M.A.; Yousefi, G.R. Conjugate active and reactive power management in a smart distribution network through electric vehicles. *Sustain. Energy Grids Netw.* **2020**, *22*, 100344. [CrossRef]
17. Partovi, M.; Esmaeili, S.; Aein, M. Increasing the penetration of electric vehicles in distribution networks using optimal charging/discharging control and reactive power support in the presence of nonlinear loads. *Int. Trans. Electr. Energy Syst.* **2022**, *2022*, 3838113. [CrossRef]
18. Partovi, M.; Esmaeili, S.; Aein, M. Probabilistic optimal management of active and reactive power in distribution networks using electric vehicles with harmonic compensation capability. *IET Gener. Transm. Distrib.* **2022**, *16*, 4304–4320. [CrossRef]
19. Yang, X.; Jiang, W.; Ma, J.; Xu, D.; Zhang, C.; Yang, Y.; Xu, Z. Flexibility provision by virtual power line and soft open point in AC/DC distribution systems. *Int. J. Electr. Power Energy Syst.* **2025**, *166*, 110528. [CrossRef]
20. Zhao, J.; Qu, J.; Ji, H.; Xu, J.; Hasanien, H.M.; Turky, R.A.; Li, P. Robust operation of flexible distribution network with large-scale EV charging loads. *IEEE Trans. Transp. Electrif.* **2024**, *10*, 2207–2219.
21. Nayak, A.; Maulik, A.; Das, D. An integrated optimal operating strategy for a grid-connected AC microgrid under load and renewable generation uncertainty considering demand response. *Sustain. Energy Technol. Assess.* **2021**, *45*, 101169. [CrossRef]
22. Gangil, G.; Saraswat, A.; Goyal, S.K. An uncertainty aware optimal energy management model for smart distribution networks contemplating reactive support from VRE and energy storage systems. *IEEE Access* **2025**, *13*, 91423–91450. [CrossRef]
23. Ma, Y.; Dong, X.; Yang, P.; Liu, Z.; Wang, Y.; Lu, T. Robust optimization model of flexible distribution network considering source-load uncertainty. *Electr. Power Syst. Res.* **2023**, *223*, 109698. [CrossRef]
24. Useche-Arteaga, M.; Gil-González, W.; Gomis-Bellmunt, O.; Cheah-Mane, M.; Lacerda, V. Robust energy management in active distribution networks using mixed-integer convex optimization. *Electr. Power Syst. Res.* **2025**, *241*, 111367. [CrossRef]
25. Seyedeh-Barhagh, S.; Abapour, M.; Mohammadi-Ivatloo, B.; Shafie-Khah, M.; Laaksonen, H. Optimal scheduling of a microgrid based on renewable resources and demand response program using stochastic and IGDT-based approach. *J. Energy Storage* **2024**, *86*, 111306. [CrossRef]
26. Chen, Q.; Wang, W.; Wang, H.; Dong, Y.; He, S. Information gap-based coordination scheme for active distribution network considering charging/discharging optimization for electric vehicles and demand response. *Int. J. Electr. Power Energy Syst.* **2023**, *145*, 108652.
27. Gholami, K.; Azizivahed, A.; Arefi, A.; Li, L. Risk-averse Volt–VAr management scheme to coordinate distributed energy resources with demand response program. *Int. J. Electr. Power Energy Syst.* **2023**, *146*, 108761.

28. Gao, H.; Wang, L.; Liu, J.; Wei, Z. Integrated day-ahead scheduling considering active management in future smart distribution systems. *IEEE Trans. Power Syst.* **2018**, *33*, 6049–6061. [CrossRef]
29. Baran, M.E.; Wu, F.F. Network reconfiguration in distribution systems for loss reduction and load balancing. *IEEE Trans. Power Deliv.* **1989**, *4*, 1401–1407. [CrossRef]
30. Wang, Z.; Wang, J.; Chen, B.; Begovic, M.M.; He, Y. MPC-based voltage/Var optimization for distribution circuits with distributed generators and exponential load models. *IEEE Trans. Smart Grid* **2014**, *5*, 2412–2420.
31. Kuang, Z.; Liu, G.; Lu, H.; He, Y. Assessment and influencing factor analysis of multi-type load acceptance capacity of active distribution network. *Electronics* **2025**, *14*, 1566. [CrossRef]
32. Hamidi, A.; Golshannavaz, S.; Nazarpour, D. D-FACTS cooperation in renewable integrated microgrids: A linear multiobjective approach. *IEEE Trans. Sustain. Energy* **2019**, *10*, 355–363.
33. Zhang, Y.; Liu, Z.; Wang, F.; Chen, Z. Distributed power allocation scheme with prescribed performance and intermittent dynamics for BESSs with discharge rate constraints in microgrids. *IEEE Trans. Syst. Man Cybern. Syst.* **2025**, *55*, 1948–1959.
34. Zhang, Y.; Liu, Z.; Chen, Z. A PI+R control scheme based on multi-agent systems for economic dispatch in isolated BESSs. *IEEE/CAA J. Autom. Sin.* **2024**, *11*, 2154–2165.

Disclaimer/Publisher's Note: The statements, opinions and data contained in all publications are solely those of the individual author(s) and contributor(s) and not of MDPI and/or the editor(s). MDPI and/or the editor(s) disclaim responsibility for any injury to people or property resulting from any ideas, methods, instructions or products referred to in the content.